RSC Advances

PAPER

View Article Online
View Journal | View Issue

Cite this: *RSC Adv.*, 2026, **16**, 12856

Interpenetrating gelatin/sodium alginate hydrogel with controlled PRP lysate delivery for accelerating diabetic wound healing with reduced scarring

Fairooz Nawer,[a] Abdur Rahman,[a] Ashraful Hoque[b] and M. Tarik Arafat *[a]

Hyperglycemia induced growth factor deficiency in diabetic wounds confines the wound healing process to chronic inflammation and impairs effective healing. Platelet rich plasma lysate (PL) biomolecules (growth factors and cytokines) have shown efficacy in triggering effective wound healing signals in diabetic wounds. However, PL injection at the wound site causes early degradation of the biomolecules by the wound enzymes, underlining the necessity of a controlled biomaterial based delivery platform. In this study, an interpenetrating polymer network (IPN) hydrogel composed of natural polymers, gelatin, and sodium alginate (Gel/SA) was introduced to overcome the limitations of natural polymers and as a delivery medium for PL. The IPN was developed through simultaneous covalent crosslinking of gelatin and ionic crosslinking of sodium alginate, forming a dense network. The Gel/SA IPN hydrogel provides accessible favorable functional groups of the polymers which offer better swelling, water retention and more controlled diffusion dominated PL delivery than the conventional Gel/SA hydrogels. The Gel/SA IPN hydrogel exhibited the required wound dressing properties, such as swelling properties, gel fraction (80%), water retention capacity, water vapor transmission rate, hemolysis, blood clotting, and antibacterial properties. The ATR-FTIR spectra confirmed successful IPN formation, which provided controlled network degradation, offered the sustained release (70%) of PL, and optimized their susceptibility to wound enzymes. The results showed that the Gel/SA@PL hydrogel provided effective blood clotting and wound healing properties with enhanced growth factor mediated hemostasis, re-epithelialization, adipocyte formation to regulate granulation tissue formation, uniform collagen deposition, and minimal scar formation in the diabetic wound model.

Received 16th December 2025
Accepted 17th February 2026

DOI: 10.1039/d5ra09743f

rsc.li/rsc-advances

1 Introduction

Diabetic complications such as hyperglycemia, neuropathy, vascular abnormalities, chronic inflammation, *etc.*, contribute to the formation of chronic diabetic wounds. Hyperglycemia can induce malfunctioning skin cells, excessive reactive oxygen species (ROS) production, and peripheral neuropathy, resulting in compromised re-epithelialization, vascular dysfunctionalities, and excess pressure at skin surfaces. These phenomena eventually lead to impaired wound healing with compromised tissue regeneration in diabetic wounds. Peripheral neuropathy increases the risk of diabetic foot ulcers by escalated pressure at the bottom surface of the foot, reduced blood flow, repeated tissue injury, biofilm formation by microbes, low activity of growth factors and cytokines, and large amounts of inflammatory cells at the wound site, causing chronic inflammation. Extended chronic inflammation increases protease activity, which causes proteolysis of growth factors and the extracellular matrix (ECM), preventing the wound healing progression from inflammation to proliferation and trapping the healing in a chronic inflammation loop.[1,2]

To treat chronic wounds such as diabetic foot ulcer (DFU), molecular therapies are the most effective approach. However, finding a proper way to provide molecular therapies remains challenging.[3] Growth factors such as platelet derived growth factor (PDGF), vascular endothelial growth factor (VEGF), fibroblast growth factor (FGF), epidermal growth factor (EGF), hepatocyte growth factor (HGF), transforming growth factor (TGF-β), keratinocyte growth factor (KGF), angiopoietin-I (ANG-I), stromal cell derived factor (SDF-1α), and cytokine tumor necrosis factor (TNF α-β) have demonstrated the ability to boost diabetic wound healing, alleviating inflammation, and vascular problems in diabetic wounds. FDA approved the clinical application of recombinant human platelet-derived growth factor (rh-PDGF-BB) for treating diabetic foot ulcers, and other single growth factor applications such as recombinant human basic fibroblastic growth factor (rh-bFGF) or recombinant human vascular endothelial growth factor (rh-VEGF-A) for

[a]*Department of Biomedical Engineering, Bangladesh University of Engineering and Technology, Dhaka-1205, Bangladesh. E-mail: tarikarafat@bme.buet.ac.bd; Tel: +880255167100 ext. 6133*

[b]*Department of Transfusion Medicine, National Institute of Burn and Plastic Surgery, Dhaka, Bangladesh*

wound healing have also been explored. However, compared to single growth factor application, PL provides a more advantageous platform where symbiotic combined activities of multiple growth factors in the wounded area can significantly enhance wound healing.[4,5] PL is an acellular preparation comprised of platelet released growth factors, proteases and protease inhibitors, antimicrobial proteins, and cytokines, among various other elements.[6–8] It has been found in a study that subcutaneous infiltration of PRP in cutaneous wounds in dog demonstrated enhanced wound healing dynamics including high collagen deposition and reduction of scar formation.[9]

However, the topical application of such growth factors for clinical chronic wound treatment has exhibited unfavorable results, such as the dilution of growth factors by wound exudates.[10] Topical application or intradermal injection are two ways to accomplish direct delivery; nevertheless, the bioactivity is only temporary due to proteolysis and undermining support. For instance, angiogenesis cannot be sustained by a considerable infusion of numerous growth factors. Biomaterial based delivery can be accomplished by adding growth factors to ECM like hydrogels, scaffolds, or particles that can offer proteolytic protection and structural support while still retaining the bioactivity of growth factors.[11] An ideal wound dressing should have tunable degradation to resemble the wound healing timeline, high swelling capacity, and water retention properties to absorb chronic wound exudate and maintain appropriate moist wound bed, conformity, and nonadherence to the wound to avoid pain during dressing removal. While widely available wound dressings composed of fibers, films, foams, and nanoparticle based topical formulations fail to meet these criteria, hydrogel stands out with its attractive features, such as antioxidant properties, tunable biodegradability, flexibility, mechanical strength, porosity, efficient loading of molecules, *etc.*[12,13]

Gelatin primarily consists of the remains of three amino acids: glycine (arranged every third unit), proline, and 4-hydroxyproline, and offers good biodegradability, biocompatibility, and increased pyrrolidines, forming a strong gel.[14] Gelatin molecules can form an electronic interaction based on the charge located over its polymer backbone and the acidic/essential nature of the growth factors in the presence of collagenase secreted by the damaged tissue.[15] This interaction between gelatin and growth factors immobilizes the growth factors in the network meshes, and the growth factors are released by controlled degradation of gelatin based hydrogels. Gelatin based biomaterials combined with different synthetic polymers to incorporate single growth factors were studied for delivering growth factors to accelerate wound healing in chronic wounds.[3] Gelatin based hydrogel provided sustained release of fibroblast growth factor, which promoted angiogenesis and granulation tissue formation more efficiently than the topical application of the growth factor.[16] Pure gelatin based hydrogels exhibit low tensile strength and mechanical stability, compromising their eligibility for wound dressing applications.[17] It has been exhibited in a study that gelatin/alginate composite can form a stable structure with H bonding and depicts promising potential in encapsulating epidermal growth factor (EGF) through electrostatic interaction.[18] Sodium alginate can introduce many advantageous properties to the gelatin sheet hydrogels, such as improved mechanical stability, water vapor transmission capacity, hydrophilicity, bioadhesion, immunogenicity, and protein absorption quality, triggering re-epithelialization and granulation tissue formation for accelerated wound closure.[19–21] Sodium alginate can covalently bind with the adhesion peptides of growth factors, promoting the controlled release of growth factors from its network.[22] Studies have shown that gelatin/sodium alginate scaffolds play a significant role in reducing inflammation and collagen reconstruction and in promoting scar reduction.[23,24] Although gelatin/alginate hydrogel combination has been studied with different delivery molecules and functional molecules to trigger favorable molecular activity for wound healing applications, this combination has not yet been studied for delivering multiple growth factors.[25,26] This is because of their poor mechanical properties and the structural network instability. Therefore, novel dual networking or combination with synthetic polymers has been studied to overcome these challenges.[27]

Studies have shown that semi IPN and double network gelatin/sodium alginate hydrogels hold great potential for tissue engineering applications. A study compared alginate semi IPN hydrogel with alginate/gelatin IPN for organ bioprinting and found that semi IPN hydrogel was mechanically unstable with poor integrity.[28] Another study depicted that double network of gelatin/sodium alginate hydrogel offers high stiffness and toughness which are more suitable for cartilage tissue engineering rather wound healing applications.[29] Hence, studies explored gelatin/sodium alginate IPN hydrogel networks through Schiff base or zero length crosslinking of gelatin and ionic or UV crosslinking of sodium alginate for skin tissue regeneration.[30,31] The interpenetrating network (IPN) development strategy can be adopted as a dual network technology, as it can provide better mechanical properties along with high swelling, permeability, and tunable drug release.[32] An IPN comprises physically entangled crosslinked polymer networks without any internetwork chemical bond.[33] IPN possesses a denser network than a single polymer network, which offers properties such as good mechanical stability, favorable swelling capacity, and tunability of drug loading and release kinetics through controlled porosity and degradation.[32] A dual crosslinked gelatin/sodium alginate based IPN hydrogel system loaded with berberine demonstrated a highly porous network resulting in high swelling capacity along with good biocompatibility, antibacterial properties, and controlled drug release, enhancing its scope in wound dressing applications.[34] Another study on physically crosslinked gelatin/sodium alginate hydrogel, which formed an IPN of polymers crosslinked by alginic acid and hydrogen bonds, revealed excellent mechanical properties, stability in different pH solutions, and self healing properties, expanding its application horizon in different biomedical technologies and biosensors.[35] IPN hydrogel networks have been proven to be an excellent ECM structure for releasing growth factor rich PRP. A study fabricated an IPN consisting of a fibrinogen network from PRP and a sodium alginate network to entrap growth factors released from the activated platelets in PRP. PRP gel can be damaged in different

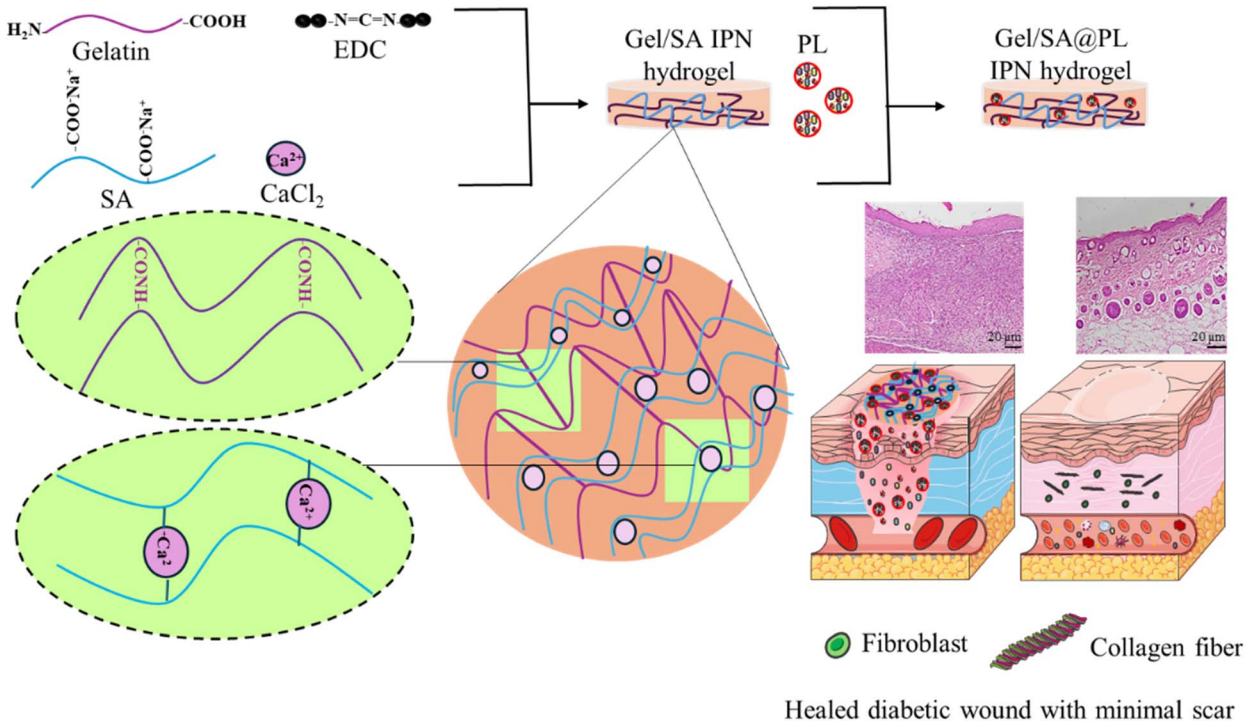

Fig. 1 Human PL was incorporated into the Gel/SA IPN hydrogel network to accelerate diabetic wound healing. EDC triggered the crosslinking of gelatin polymer chains, and sodium alginate polymer chains were crosslinked by Ca^{2+} ions. Individual crosslinked polymer chains coexisted in the IPN to form the hydrogel. PL loaded Gel/SA@PL IPN hydrogel dressing was applied topically to a diabetic mice wound model, which closed the wound with minimal scar formation. Figure was partially adapted from Smart-Servier Medical Art.

physiological conditions, leading to an increased clearance rate and a short half life of growth factors, compromising its application in wound healing. Compared to single network PRP gel, this double network hydrogel provided excellent self healing properties and sustained release of entrapped growth factors.[36]

Pure gelatin and sodium alginate have some limitations in their swelling capacity and mechanical stability.[37] Fabricating an IPN structure which consists of these two polymers can compensate for these limitations. IPN hydrogels keep the hydrophilic groups of the polymer chains unoccupied which contribute to the water uptake in the system, increasing the swelling capacity of the network. The dense polymer network of the structure limits solvent transport with fewer aqueous channels which restrict water loss and facilitates controlled degradation with increased solvent permeation.[38,39] The incorporation of sodium alginate as a secondary network in the IPN offers controlled release of the molecule due to polymer's ionizable group and pH dependent swelling behavior along with the structure's favorable diffusion pathways for the entrapped molecule.[38,39] Therefore, the IPN hydrogel network holds great potential for efficient encapsulation and controlled release of PL. Although gelatin/sodium alginate IPN exhibited promising drug release kinetics, it has not yet been studied for the release of growth factors. Considering the excellent features of gelatin/sodium alginate IPN and its prospect of overcoming the challenges of pure natural polymer based hydrogels, a gelatin/sodium alginate IPN hydrogel dressing was fabricated for the controlled release of PL to explore its advantages in treating chronic diabetic wounds (Fig. 1).

2 Materials and methods

2.1 Materials

Porcine gelatin and EDC (1-ethyl-3(3-dimethylaminopropyl) carbodiimide) were purchased from Sigma Aldrich, India. Sodium alginate (the viscosity of 2% solution is 3200 mPa s at 25 °C) and Calcium Chloride were obtained from Loba Chemie, India. All other chemical components are reagent grade.

2.2 Methods

2.2.1 Fabrication of Gel/SA hydrogel. 10% (w/v) porcine gelatin and 2% (w/v) Sodium Alginate were mixed in 10 mL DI. The solution was stirred at 65 °C for 3–4 h with high rpm followed by low rpm after the gelatin was mixed using a magnetic stirrer. The solution was poured into a small 2 cm diameter Petri dish and kept at 4 °C for 24 h. A crosslinker solution was made using 3% EDC and 8% $CaCl_2$. These two components were dissolved in Ethanol. After 24 h, the solution in the Petri dish formed a gel, which was demolded and immersed in the crosslinker solution for another 24 h at the same temperature as before. Hydrogel was formed and collected by washing it with DI several times.

2.2.2 Extraction of PL. To extract PL human blood was collected in accordance with the Declaration of Helsinki and applicable national regulations. The experiments were

approved by the ethics committee of the National Institute of Burn & Plastic Surgery under approval number NIBPS-February24/03. Informed consents were obtained from human participants of this study. The blood underwent plasmapheresis to yield platelet concentrate with sample density of 3×10^{11} cells per μL. Platelet concentrates were exposed to two repeated freeze–thaw cycles (frozen at −80 °C for 18 h and thawed at 37 °C for 30 min) to trigger platelet lysis and activation of its biomolecules, as shown in Fig. 2(a). The obtained PL was diluted with DI in a 1 : 1 ratio.

2.2.3 Fabrication of PL incorporated Gel/SA@PL hydrogel. The solution was poured into a small 2 cm diameter Petri dish for obtaining spherical shape and kept at 4 °C for 24 h.

2.3 Characterizations

2.3.1 Attenuated total reflectance fourier transform infrared (ATR-FTIR) spectroscopy. The chemical structure and network bond among gelatin, sodium alginate, and PL was observed by analyzing the characteristic peaks of pure gelatin hydrogel, sodium alginate hydrogel, liquid PL, Gel/SA hydrogel, and Gel/SA@PL hydrogel using Nicolet iS5 FTIR Spectrometer (Nicolet Instrument Corporation, WI, USA) in the wavelength range of 4000–500 cm^{-1}. The measurements were taken using OMNIC spectra software. The test was done in a silent room to reduce background noise, and the diamond tip was properly rinsed with propanol before testing.

2.3.2 Swelling. Pre weighed samples of the Gel/SA@ PL and Gel/SA hydrogel composites were dissipated in 10 mL of PBS, which were preserved in 20 mL glass vials for 24 h at 37 °C. The composite hydrogels were removed from the PBS and weighed after soaking up excessive water on absorbent tissue paper. The following equation was used to determine the water uptake:

$$\text{Swelling}(\%) = \frac{W_{\text{wet}} - W_{\text{dry}}}{W_{\text{dry}}} \times 100$$

W_{wet} and W_{dry} refer to the weight of wet and dry composite gel, respectively. Swelling experiments were conducted three times for upconverting hydrogel composites.

2.3.3 Degradation. The *in vitro* hydrolytic degradation of the hydrogel was measured after the swelling test. The effect of salt ions and water on the gelatin and alginate chain disentanglement was analyzed using PBS of pH 7.[40] The samples were submerged in PBS at 37 °C for 5 days, followed by oven-drying at 60 °C to disrupt the network at the polymer level, and weights were taken in several time intervals.

$$\text{Degradation}(\%) = \frac{W_{\text{i}} - W_{\text{d}}}{W_{\text{i}}} \times 100$$

W_{i} and W_{d} indicate the hydrogel's initial and final dry weights after degradation, respectively.[41]

2.3.4 Gel fraction. The pre weighed hydrogel pieces (1×1 cm^2) were dried at 40 °C for 24 h. The dried hydrogel pieces were immersed in distilled water for 48 h at 37 °C to reach swelling weight. The part of the remaining hydrogel was again oven-dried at the same temperature for another 24 h to obtain the dried crosslinked structure. The hydrogel became a dried film, and it was weighed. The gel fraction was calculated using the following formula:[42]

$$\text{Gel fraction}(\%) = \frac{W_{\text{d}}}{W_{\text{i}}} \times 100$$

W_{d} and W_{i} indicate the final dried film weight and the initial dried hydrogel weight, respectively.

2.3.5 Water retention capacity. The hydrogel samples were swollen in DI water for 24 h. After the removal of excess surface water, the initial wet weight (W_{o}) of the hydrogel was taken. The samples were then kept at room temperature with 60% relative humidity for 24 h, and the final weight (W_{t}) was taken.

$$\text{Water retention capacity}(\%) = \frac{W_{\text{t}}}{W_{\text{o}}} \times 100\%$$

2.3.6 Water vapor transmission rate (WVTR). The water vapor transmission rate was calculated following the method described in ref. 43. A spherical shaped, 15 mm diameter hydrogel was attached to the top of the test tube filled with 5 mL water with an air gap of 6 mm. Hydrogel with the test tube was kept in an incubator at 37 °C with a relative humidity of 35%. A control test tube with hydrogel attached to the top of the tube with no water was used, and the difference between the weight of the test tubes with water and the control was taken as the water weight of the test tube. Taking the water weight data of the test tube for days 1, 2, and 4, WVTR was obtained from the following equation:

$$\text{WVTR} = \frac{\Delta W}{tA} \text{ g per m}^2 \text{ per day}$$

Here, ΔW is the weight loss of water, t is time in days, and A is the test area of the sample (m^2).

2.3.7 Hemolysis. 2% RBC was mixed with 50 mL PBS to make RBC suspension. 0.1 mL detergent, Triton X-100, was dissolved with 9.9 mL DI and was kept at 37 °C in an incubator for a few minutes to dissolve the detergent in DI properly. 10 mg of hydrogel was immersed in 10 mL of RBC suspension in a centrifuge tube. Positive control was prepared using 9 mL RBC suspension with 1 mL Triton X-100.10 mL RBC suspension was used as a negative control. All three centrifuge tubes were kept at 37 °C in an incubator for 1 h. After 1 h, tubes were sealed with a lid and paraffin and centrifuged at 3000 rpm for 10 min at room temperature. After centrifugation, the supernatant of all three samples was separated, and the absorbance of the supernatant was measured at 545 nm. The hemolysis ratio was calculated using the absorbance values of the sample, positive control, and negative control supernatants using the following equation:

$$\text{Hemolysis ratio}(\%) = \frac{A_{\text{s}} - A_{\text{n}}}{A_{\text{p}} - A_{\text{n}}} \times 100$$

A_{s}, A_{n} & A_{p} indicate, the absorbance of the sample, negative control, and positive control, respectively.[44,45]

2.3.8 Blood clotting index (BCI). 30 mg hydrogel samples were incubated at 37 °C for 10 minutes. 100 μL of whole blood was placed on the surface of the incubated hydrogel. After 10

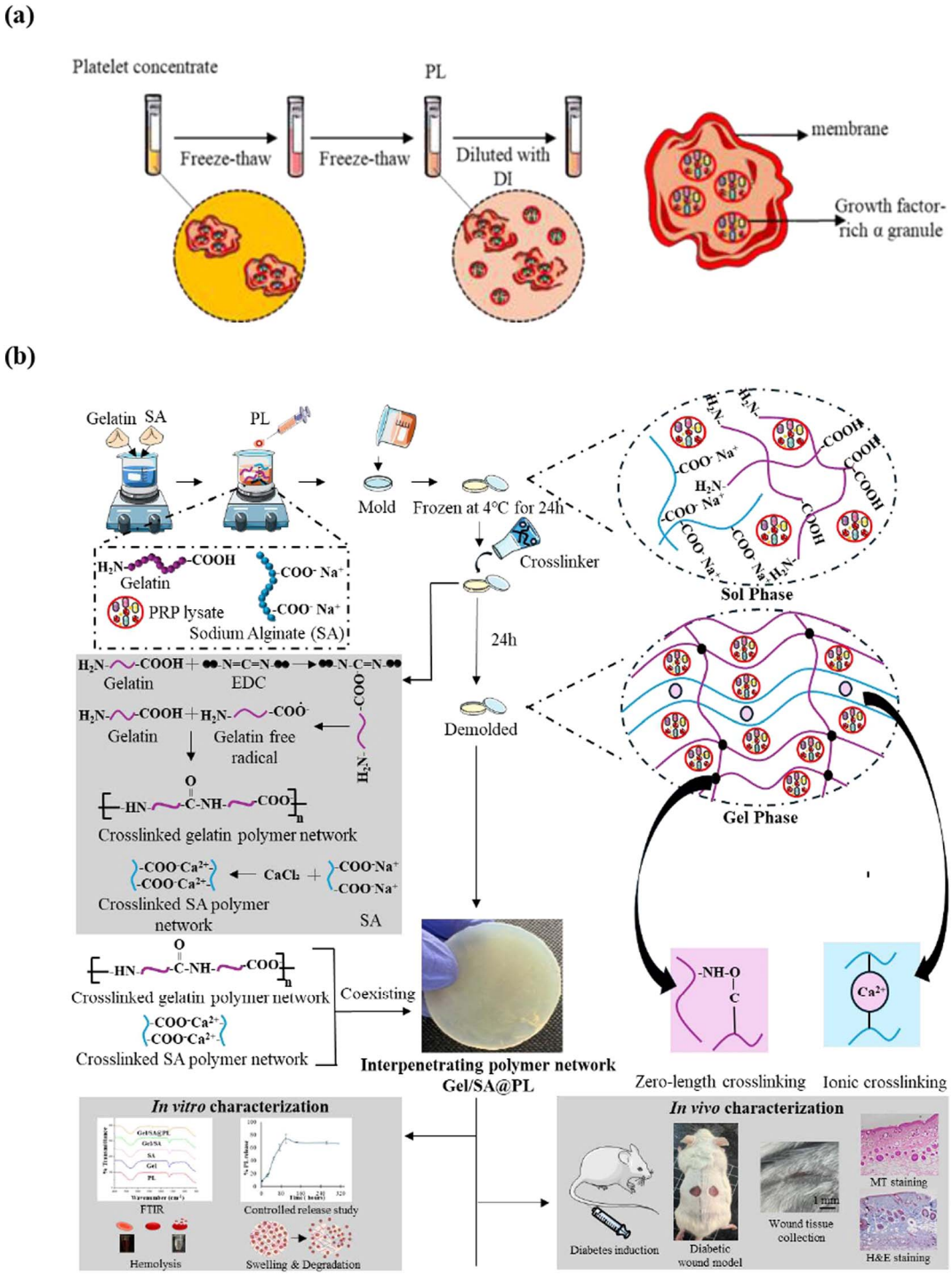

Fig. 2 Experimental workflow of PL extraction, Gel/SA@PL IPN hydrogel fabrication and characterization techniques. (a) Platelets were degraded by freeze–thawing platelet concentrate to release the growth factor rich α granules in the liquid PL. Repeated freeze thawing converts the platelets into cell-free, soluble lysate which ensures direct access to the growth factors while preventing the infection risk associated with the cellular debris of platelets. (b) A sol–gel method was adopted to develop the hydrogel where a sol precursor of gelatin and sodium alginate mixture was prepared at room temperature, and PL was added dropwise to the precursor. The gel phase of the polymer solution was triggered by storing the solution in a mold at 4 °C. In this phase, two independent crosslinking occurred simultaneously. Gelatin and sodium alginate polymer chains underwent zero length crosslinking and ionic crosslinking respectively to form the IPN of gelatin and sodium alginate polymer chains and physically entrapped the PL α granules inside the IPN meshes. This network provides efficient mechanical stability to the hydrogel dressing while offering controlled release of PL growth factors during wound healing.

minutes of incubation, a sample with 30 mL DI water was added to the blood clotted samples and centrifuged at 1000 rpm for 1 minute to lyse the unclotted RBC. The absorbances of the supernatant fluid with control of whole blood without a sample were measured using a UV spectrophotometer.

$$\mathrm{BCI} = \frac{A_{\mathrm{sample}}}{A_{\mathrm{ref}}} \times 100\%$$

A_{sample} and A_{ref} indicated the absorbances of the supernatant fluid of the sample and the control, respectively.[46]

2.3.9 RBC attachment. 200 μL of 10% RBC suspension was added to the samples, and the samples with RBC suspension were then incubated at 37 °C for 1 hour. The supernatant RBC suspension was separated, and the RBC attached samples were rinsed three times with 0.9% NaCl and then washed with 0.2 M PBS (pH 7). The samples were then immobilized in 2.5% glutaraldehyde for 2 hours at 4 °C, followed by dehydration using 20%, 40%, 60%, 80%, and 100% ethanol, respectively. After air drying at room temperature for 1 month, the samples were observed using a scanning electron microscope (Zeiss Sigma 300 VP FESEM) after sublimation for half an hour, and platinum deposition.[46]

2.3.10 *In vitro* bacterial response study. This study was performed following the method described in ref. 47. Briefly, 20 μL of *Staphylococcus aureus* and *Escherichia coli* suspension with PBS of pH 7.4 was dispensed onto the hydrogel placed above the nutrient agar culture medium. A control was prepared by dispersing the bacteria onto the gauze placed above the agar culture medium. Both Gel/SA and Gel/SA@PL hydrogels were analyzed for bacterial growth after incubating for 24 h at 37 °C. The bacterial growth was analyzed using the colony growth on the hydrogel surface, and the penetration study was performed by counting the bacterial colony growth in the agar culture medium.

2.3.11 *In vitro* PL release study. Wavelength scanning was performed for PL, and an absorbance peak at 280 nm was found. This wavelength value also coincided with a study that analyzed the PL release from nanoparticle loaded hydrogels.[48] The standard curve of PL was used to determine the released amount of PL in the PBS using hydrogel samples. 0.1 g hydrogel samples were placed in 5 mL PBS (pH 7) solution and were incubated at 37 °C. 3 mL of the solutions were taken from each sample containing solution at predefined intervals for measuring the absorbance using a UV spectrophotometer (Shimadzu UV-3100) at 280 nm and placed in the primary solution again. The standard curve of PL was used to determine the released amount of PL in the PBS using hydrogel samples.

The PL release data were analyzed using different kinetic models (Anagha *et al.*, 2019). These models included the Korsmeyer Peppas model $\left(\frac{C_t}{C_\infty} = K_{k_p} t^n\right)$ and the Higuchi model ($M = K_h t^{1/2}$), as well as the zero-order model ($M = k_o t$) and the first-order model ($\ln(1 - M) = -k_1 t$). In these equations, C_t represents the drug amount released at a specific time point, t, C_∞ is the drug amount at the final measurement time, and M denotes the drug amount released at time t. The rate constants for each model, namely K_{k_p} for Korsmeyer–Peppas, K_h for Higuchi, k_o for zero-order, and k_1 for first order, were also involved. The release exponent (n) and the correlation coefficient (R^2) were subsequently calculated from the analysis.

2.3.12 *In vivo* wound healing assessment. 42 Swiss albino mice were acquired from the animal facility of the Department of Biomedical Engineering, BUET. All the experimental studies were approved by The Animal Ethics Committee of the Biomedical Engineering Department of Bangladesh University of Engineering & Technology under the protocol number 2024/BME/04.

Diabetes was induced in Swiss albino mice with a weight between 30–35 g by injecting streptozotocin intraperitoneally at multiple low doses for five days. The protocol was obtained from ref. 49. Briefly, the mice were fasted for 4 hours before the injection. The mice were injected with 0.32% streptozotocin dissolved in citrate buffer for five days, followed by access to 10% sucrose water and food. The fasting blood sugar of the mice was measured for 5, 10, 15 and 20 days.

Later, diabetic mice weighing between 30–35 g were selected for the experiments and were anesthetized with an optimum dose of ketamine hydrochloride before the operation—a biopsy tool induced circular wounds at the dorsal side of the mice. The ulcer wound resembles the chronic wound developed in diabetic patients. The moist samples obtained after 24 hours of crosslinking were sterilized for the *in vivo* wound healing assessment. Samples were sterilized by rinsing them with 70% ethanol and washed with PBS thrice to remove excess ethanol.

The sterilized samples were secured with Tegaderm on the circular wound of diabetic mice. Hydrogel samples were removed after 5 days, and the wounds were secured with Tegaderm only. The control mice wound was treated with gauze only. Gauze treated, Gel/SA hydrogel treated, and Gel/SA@PL hydrogel treated wound tissues were collected after 3 and 7 days. The wound tissues were fixated in 10% formalin for 24 h. Then, the sample was dehydrated using a graded series of propanol of different concentrations for 2 h each and embedded in paraffin. 5 μm thick tissue slices were stained with hematoxylin & eosin (H & E) and Masson's trichrome (MT) and visualized by optical microscope. H & E was utilized to determine the epithelial gap, blood vessels per mm^2 of area, adipocytes per mm^2 of area, and epithelial thickness of the tissue wound site using ImageJ software. MT staining of wound tissues was analyzed for quantification of collagen and scar index using ImageJ.[50] Wound closure rate and scar index were determined using the following equations:

$$\text{Wound closure rate} = \frac{\text{final wound area} - \text{initial wound area}}{\text{initial wound area}} \times 100\%$$

$$\text{Scar index} = \frac{\text{scar area}}{\text{dermal thickness}} \times 100\%$$

2.4 Statistical analysis

All the experiments were executed in triplicate, and statistical analysis was performed with one way ANOVA followed by Tukey's honestly significant difference (HSD) test with p values of 0.001, 0.01, 0.05.

3 Results and discussions

3.1 Formation mechanism of Gel/SA@PL IPN hydrogel

The IPN formation of the Gel/SA@ PL hydrogel was confirmed by attenuated total reflectance fourier transform infrared (ATR-FTIR) spectroscopy. As shown in Fig. 3(c), The ATR-FTIR spectra of PL, pure gelatin hydrogel, pure sodium alginate hydrogel, Gel/SA hydrogel, and Gel/SA@PL hydrogel have been collected to distinguish the structure specific chemical signature of the IPN hydrogel. All the compounds exhibited –OH bond stretching vibration absorption peaks in the range of 3000–3600 cm^{-1}. Gelatin was characterized by the bending vibration of the –NH group (amide II band) and the stretching vibration of C═O and C–N (amide I band) at 1552 cm^{-1} and 1635 cm^{-1}, respectively. These amide bands indicate covalent amide bond between polymer chains, forming a network. Fig. 3(a) illustrates the formation of the amide bond of the network. The ionized carboxyl group of gelatin reacted with the carbodiimide group of EDC to form an amine reactive intermediate, o-acylisourea. The intermediate reacted with a primary amino group of another gelatin to establish a covalent peptide bond (amide bond) between polymer chains to form a network and released EDC from the network eventually.[51] Asymmetric stretching vibration of the carboxyl group of sodium alginate polymer backbone was verified by the absorption peak at 1635 cm^{-1}. As shown in Fig. 3(b), Na^{+} ion containing carboxyl group of sodium alginate was replaced by the Ca^{2+} ions from $CaCl_2$ during ionic crosslinking. Ca^{2+} bonded with the carboxyl groups of the adjacent polymer chains and formed a network structure of its own.

The absorption peaks of the amide I bond and amide II bond of gelatin were found at 1629 cm^{-1} and 1555 cm^{-1}, respectively, in the Gel/SA hydrogel. The asymmetric stretching vibration of the carboxyl group of sodium alginate overlapped with the amide I bond of gelatin at 1636 cm^{-1} in both the Gel/SA and Gel/SA@PL hydrogel. The amide II band of gelatin was found in both the Gel/SA and Gel/SA@PL hydrogel spectra at 1558 cm^{-1}. Both the spectra of Gel/SA and Gel/SA@PL hydrogel contained the absorption peaks of their respective elements. There was no specific absorption peak indicating a bond formation between gelatin and sodium alginate polymer chains other than the peaks associated with zero length and ionic crosslinking of individual gelatin and sodium alginate polymer chains. This phenomenon is a clear indication of the fact that the crosslinking of gelatin and sodium alginate polymer chains occurred in an independent and simultaneous manner during the gel phase. Therefore, the network of gelatin and sodium alginate was physically entangled, and the sodium alginate network penetrated through the gelatin network without any chemical bond between them, forming an interpenetrating network with an aqueous medium within the network.

PL associated protein growth factors exhibited absorption peaks at 1551 cm^{-1} and 1639 cm^{-1} in the PL spectrum. The overlapping location of the amide bands of gelatin and the PL growth factors was reflected in the Gel/SA@PL hydrogel spectrum with higher intensities which denotes the physical immobilization and chemical stability of the PL associated growth factors in the IPN hydrogel.[35,52,53]

3.2 Swelling

In Fig. 4(a), both Gel/SA & Gel/SA@PL showed enhanced swelling performance with swelling percentages of 481% and 416%, respectively. The dense polymer networks of the IPN reduced the chain mobility with increased free volume for the buffer salts to enter, maintained network stability with multiple polymer chain networks and offered hydrophilic groups for increasing water uptake in the structure.[54] A previous study reported that PVA hydrogel with *Moringa oleifera* leaf extract and graphene oxide exhibited 155–171% swelling for diabetic foot ulcer application.[55] In contrast, the fully natural polymer based IPN hydrogel developed in this study demonstrated higher swelling concluding that the IPN structure improved the swelling capacity in levels comparable to synthetic polymer dressings. No significant difference was observed in the equilibrium swelling ratios of Gel/SA and Gel/SA@PL hydrogels in Fig. 4(b), indicating that the incorporation of PL associated growth factors in the interpenetrating network of the hydrogel did not compromise the structure's water absorption capacity. The high swelling capacity of natural polymer composite Gel/SA@PL hydrogel highlights the potential of cost-effective, natural polymer based IPN hydrogels as an alternative to commercial synthetic wound dressing for high exudate releasing chronic wounds such as diabetic wounds, burn wounds, *etc.*

3.3 Gel fraction

Gel fraction plays a significant role in shaping the characteristics and behavior of polymers connected through crosslinking. The value of gel content signifies the portion of the polymer that forms an unyielding gel structure due to the creation of bonds between molecules. When a hydrogel lacks crosslinks, its non crosslinked section will dissolve upon immersion in a solution, reducing its weight.[56] The outcomes of the gel fraction measurements reveal effective crosslinking, where if a significant portion of available crosslinking sites is utilized, it leads to a gel fraction of 80% or more. This suggests the successful establishment of robust networks, as there is minimal release of unlinked molecules.[57] Fig. 4(c) refers to the gel fraction of both Gel/SA hydrogel and PL loaded Gel/SA@PL hydrogel, where 80% gel fraction of Gel/SA hydrogel confirmed efficient crosslinking of two independent polymer networks of gelatin and sodium alginate. The efficient crosslinking of the polymer networks made them stable in the IPN to prevent the rupture of the structure while retaining high amount of wound exudates by the swelling process. The value of gel fraction denoted that 80% of the polymer mass was involved in developing the crosslinked network which is directly related to the amount of EDC reacted with the polymers. There were some unreacted EDC as some EDC went through side reactions, which did not lead to crosslinking. The gel fraction percentages of Gel/SA and Gel/SA@PL hydrogels exhibited no significant difference, indicating that the introduction of PL associated growth factors in the network did not impact the crosslinking of the polymer chains. Efficient crosslinking ensured the scaffold's structural integrity, consequently providing controlled PL release.

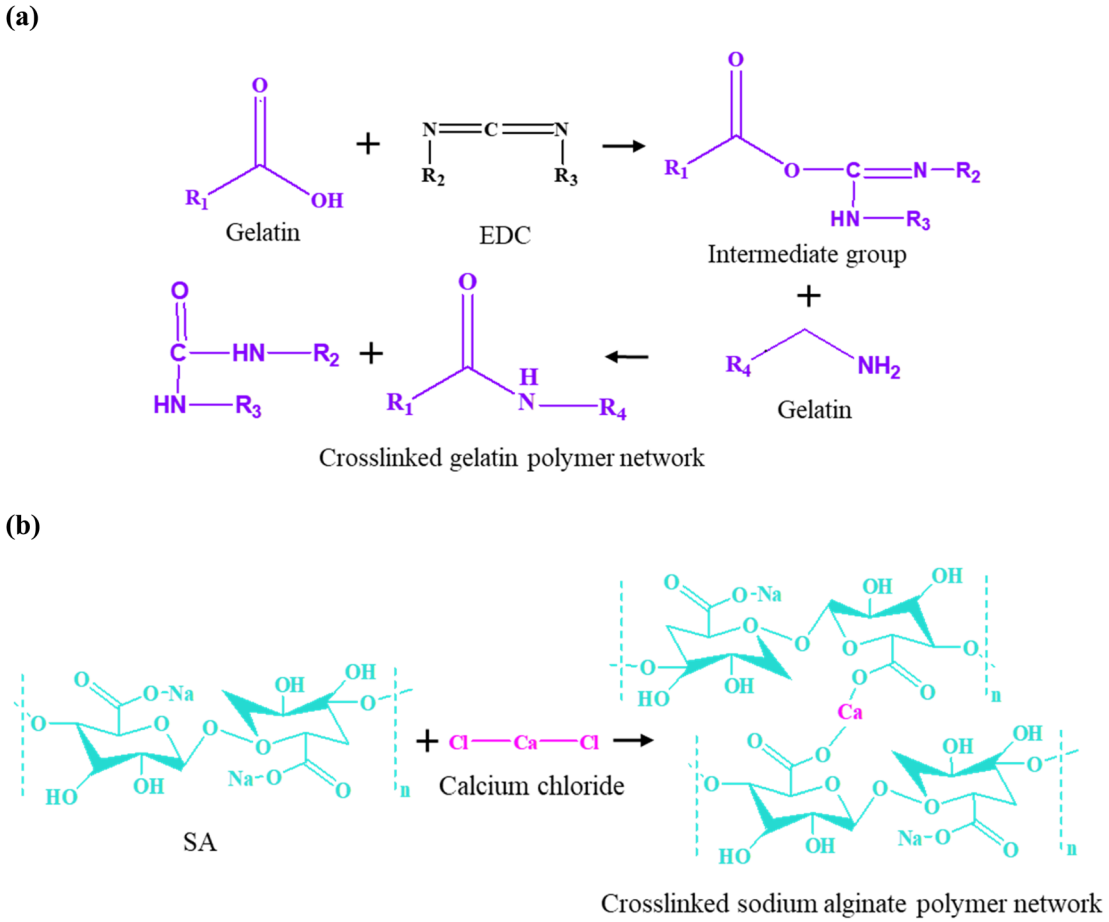

Fig. 3 Formation of IPN in Gel/SA and Gel/SA@PL hydrogel. (a) Zero length crosslinking of gelatin polymers (b) ionic crosslinking of sodium alginate polymers within the hydrogels. (c) ATR-FTIR spectra of Gelatin hydrogel (Gel), sodium alginate hydrogel (SA), PL, Gel/SA hydrogel, and Gel/SA@PL hydrogels. No H bond peak was found in either of the hydrogels, indicating IPN network formation by gelatin and sodium alginate. Gel/SA@PL hydrogel depicted the characteristic peak of PL, confirming the entrapment of PL biomolecules inside the network.

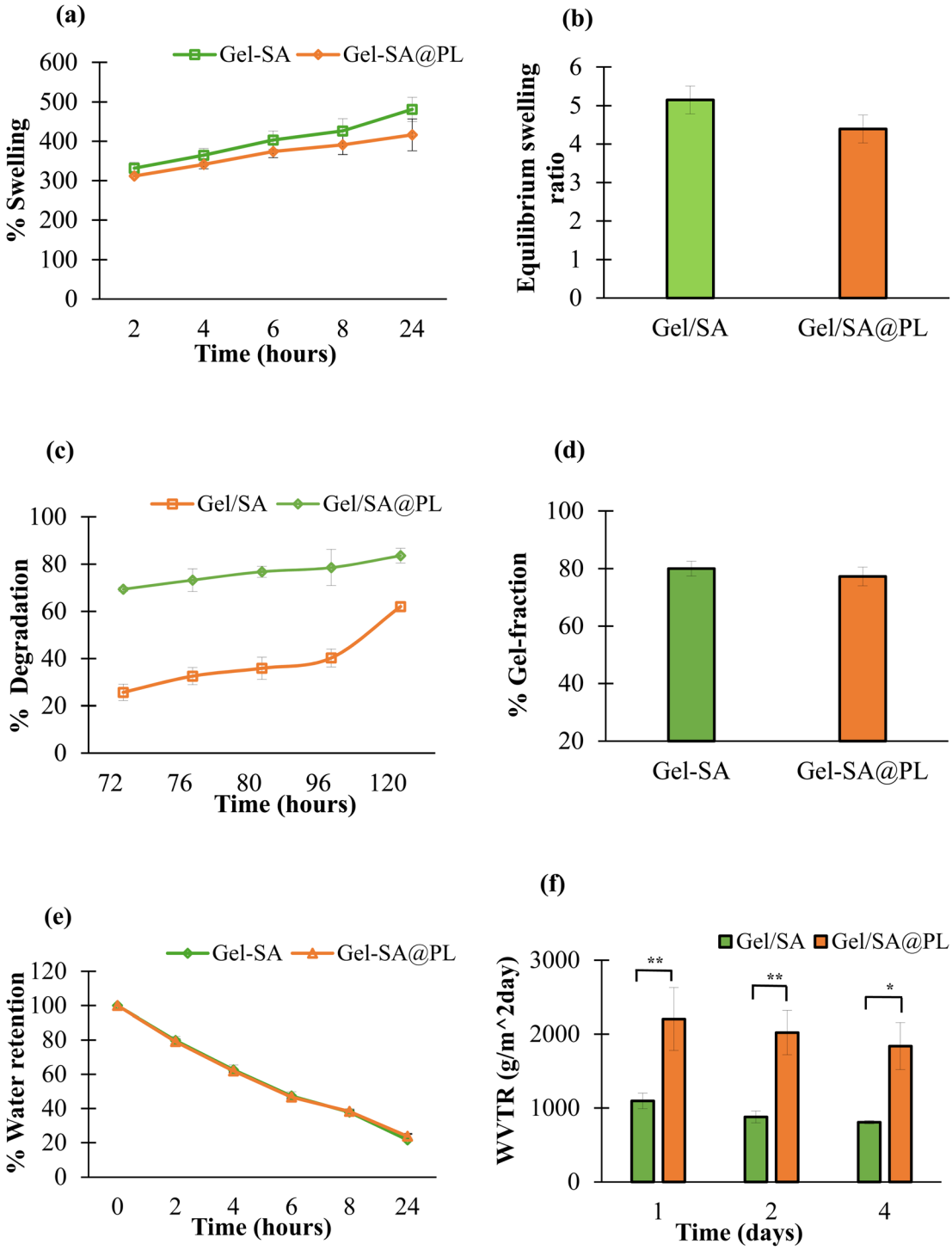

Fig. 4 Physical properties of Gel/SA and Gel/SA@PL hydrogel as wound dressings. (a and b) Swelling percentage at different intervals of time (c) degradation kinetics at different intervals of time (d) gel fraction (e) water retention properties (f) water vapor transmission rate (WVTR) of the hydrogels. WVTR values of Gel/SA@PL hydrogel were in the optimal range of WVTR of a wound dressing. Significance are denoted by *($P < 0.05$), **($P < 0.01$), ***($P < 0.001$), ($P < 0.001$).

3.4 Degradation

The swelling studies exhibited that both Gel/SA & Gel/SA@PL swelled for 24 h followed by a gradual degradation from 48 h-120 h. As illustrated in Fig. 4(d), while Gel/SA hydrogel demonstrated degradation in the range of 25–40%, Gel/SA@PL IPN hydrogel showed controlled degradation in an increased narrower range of 70–80% over a five day time window. A study showed that gelatin/sodium alginate non IPN structure provided a broader range of degradation percentage in five days.[38,58] In comparison, the IPN structure developed in this study offered accessible hydrophilic groups such as carboxylic

groups of sodium alginate and amino group of gelatin due to the lack of chemical bond between the polymer networks, facilitating the solvent permeation into the network. These chains lose their physical network due to the gel to sol transition at 37 °C and leach into the solution.[59] Both the swelling and degradation studies concluded bulk erosion of the matrix as the solvent diffusion (swelling) was faster than the polymer chain network degradation. The increase in the degradation property of the Gel/SA@PL IPN hydrogel could be due to the enhanced hydrophilic nature of the network due to the presence of PL growth factors. Effective wound management involves the utilization of wound dressing for 5–7 days. The observed controlled degradation of Gel/SA@PL hydrogel over five days at physiological condition due to the enhanced hydrophilicity of the gel/SA@PL IPN hydrogel indicates that the IPN hydrogel maintained its integrity within this clinically relevant time window which aligned with its PL release pattern.

3.5 Water retention capacity

Hydrogel's polymer network can uptake a substantial amount of water, which was previously confirmed with its swelling capacity. The water retention capacity verifies the dressing's capability of retaining the water it contained while swelling when exposed to air with dry conditions for an extended period. Fig. 4(e) shows that both the hydrogels could retain almost 23% of the water absorbed during swelling in dry conditions after 24 h. The physically entangled structure of the IPN reduced the path for water to escape, creating a 'lock-in' structure for holding a large amount of water inside the network.[38] This property can prevent the wound from dehydration, which can cause dry scabs facilitating delayed wound healing.[60] Hydrogel dressing dehydration is also kept in check by optimizing its water retention capacity, which can be essential in hydrogel dressing packaging.[34] The similar pattern of water retention capacity of Gel/SA@PL IPN hydrogel indicates that the immobilization of the PL associated growth factors in the meshes of the IPN of the hydrogels did not prevent the coexistence of water molecules inside the network.

3.6 Water vapor transmission rate (WVTR)

An ideal wound dressing must allow unobstructed oxygen circulation to reach the wound. Oxygen is critical for promoting cellular proliferation, thus expediting the healing journey. Therefore, it is preferable for hydrogels used in wound dressings to possess the ability to facilitate the passage of oxygen or gases.[61] Commercial hydrogel wound dressings have WVTR in the range of 9000–9400 g m^{-2} day^{-1}, higher than the desired range of 2000–2500 g m^{-2} day^{-1}. Hydrogels with high WVTR can result in dehydration of the wound area, which will cause the dressing to adhere to the wound surface and reduce the hydrogel size, exposing the wound edges to bacterial infection. On the other hand, hydrogel dressings with low WVTR values can lead to fluid accumulation, delayed epithelialization, disease, and scar formation. Hence, WVTR values within the range of 2000–2500 g m^{-2} day^{-1} can provide appropriate moisture to the wound, preventing wound dehydration and ensuring adequate O_2 diffusion properties.[62] Fig. 4(f) demonstrates that Gel/SA and Gel/SA@PL showed WVTR values in the range of 800–1000 g m^{-2} day^{-1} and 1800–2000 g m^{-2} day^{-1}, respectively, for four days. Gel/SA@PL exhibited higher WVTR values than Gel/SA due to the presence of favorable protein-related functional groups. The stable immobilization of PL associated growth factors in the IPN of Gel/SA@PL introduced an increased amount of protein functional groups, such as carboxyl groups, amino groups, *etc.* These functional groups increase the hydrophilicity of the hydrogel scaffold, which facilitates water vapor solubility and permeability through strong hydrophilic interaction.[63–65] WVTR values of Gel/SA@PL in the desired range indicated medium oxygen permeability through the hydrogel dressing, which has been proven to accelerate the function of epithelial cells and fibroblasts by keeping the wound moist. Moist wounds mediate rapid wound contraction and keratinocyte proliferation, resulting in enhanced re-epithelialization.[60]

3.7 Hemolysis

The hemocompatibility of the hydrogels was analyzed based on the extent of red blood cell breakdown and the release of hemoglobin upon contact with blood. As depicted in Fig. 5(a), both Gel/SA and Gel/SA@PL hydrogels exhibited hemolytic values below 2%, well within the ASTM standard F756 non-hemolytic range.[66] The significant difference (P value < 0.001) between the coloration of the supernatants of the positive control and hydrogels confirmed the excellent hemocompatibility of the hydrogels. Incorporating PL in the gelatin also showed hemolysis in the non hemolytic range, and no significant difference was observed between Gel/SA and Gel/SA@PL hydrogels. This non hemolytic property of Gel/SA@PL hydrogels proved that the hydrogels are not cytotoxic and can exhibit synergistic cellular interactions with different cells at the wound site.

3.8 Blood clotting index (BCI)

Hemostasis is one of the most critical steps in initiating effective wound healing with blood clot formation. Blood clot formation is primarily driven by the activities of functional platelets (activation, aggregation, adhesion). However, defective blood clot dissolution can hinder angiogenesis and tissue regeneration.[67] Type 2 diabetes can cause dysfunctional platelets, which exhibit hyperactivity in platelet aggregation, resulting in inefficient blood clot dissolution.[68] Human PL is enriched with functional platelets, which can ensure an effective blood clot forming process. The blood clotting index analyzes the efficacy of blood clot formation, where a lower blood clotting index means a higher blood clotting rate.[69] Fig. 5(b) concluded that both the hydrogels significantly (P value < 0.001) reduced the BCI value of the control. Gel/SA hydrogel exhibited a lower BCI value than the control confirming the gelatin and sodium alginates' contribution in blood clotting activities as mentioned in the previous studies.[24,69] The illustration in Fig. 5(c) depicts the fundamental interactions of the PL released growth factors and the platelets of the wound site, which was the primary

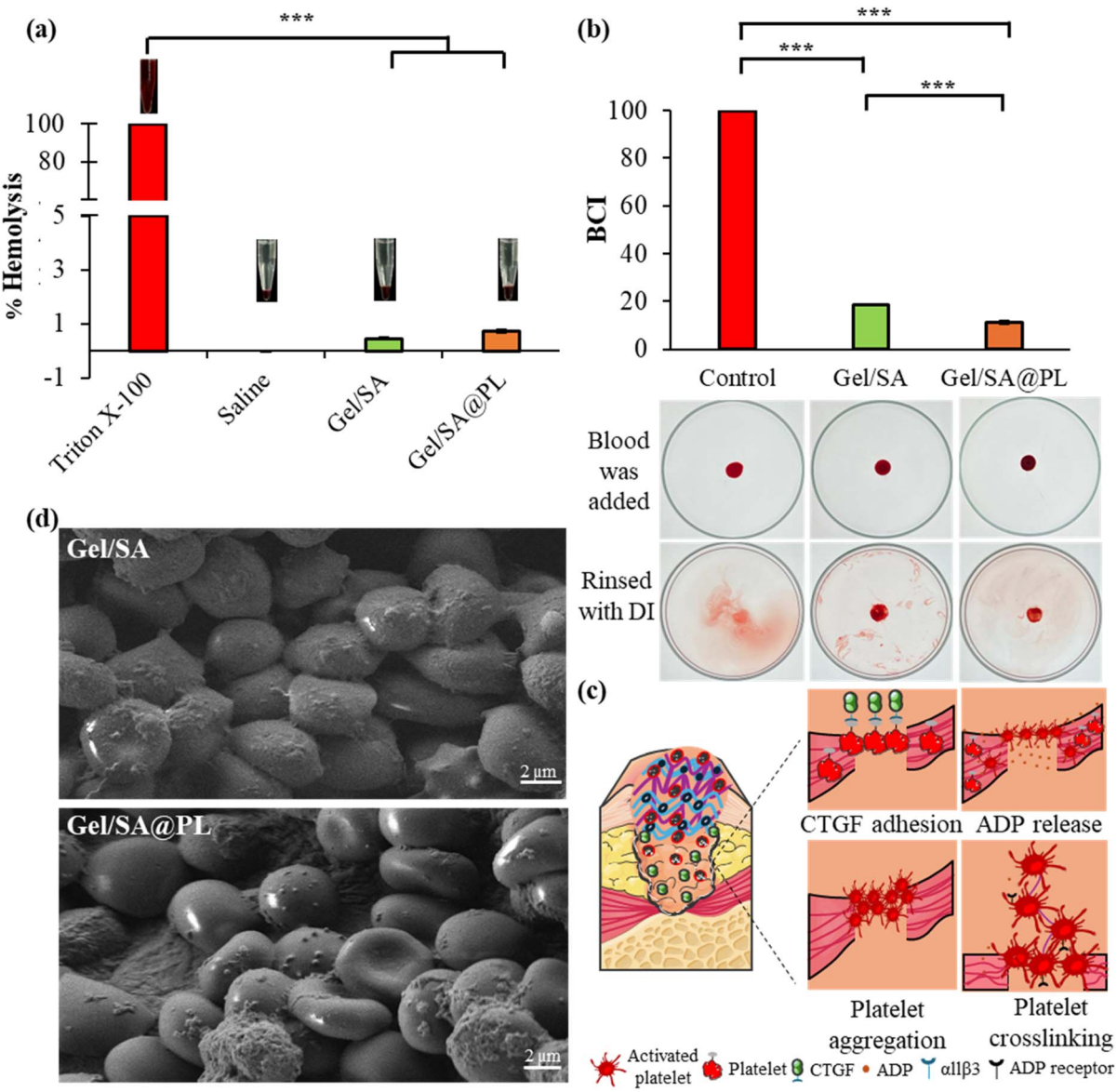

Fig. 5 *In vitro* hemocompatibility and hemostatic performance of Gel/SA and Gel/SA@PL hydrogels. (a) Quantitative hemolysis ratio analysis showed <2% hemolysis for both the hydrogels. (b) The blood clotting property was analyzed by measuring the blood clotting index (BCI), which was the lowest for the Gel/SA@PL hydrogel, indicating the fastest blood clot formation by the PL growth factor, CTGF. (c) Underlying mechanism of CTGF in platelet aggregation. (d) FESEM images of RBC attachment at Gel/SA and Gel/SA@PL hydrogel surfaces. Morphological alteration of RBC was observed in the Gel/SA hydrogel attached RBCs. Significance is denoted by *($P < 0.05$), **($P < 0.01$), ***($P < 0.001$).

rationale behind the significantly (P value < 0.001) lower value of Gel/SA@PL BCI value, shown in Fig. 5(b). Incorporation of PL in Gel/SA@PL hydrogel released the growth factor, connective tissue growth factor (CTGF), which attaches with its ligand protein, αIIβ3 to the platelets and activates the platelets to initiate platelet adhesion and aggregation, facilitating a faster rate of blood clot formation.[70,71]

3.9 RBC attachment

RBCs adhere to hydrogels due to the electrostatic interaction between the weak negative charges of RBC's surface and the positive charges of the polymer backbone of the hydrogel matrix.[72] The FESEM images of RBC in Fig. 5(d) revealed that the attached RBCs on the Gel/SA@PL hydrogel's surface maintain the proper biconcave disk morphology whereas the RBCs on the Gel/SA hydrogel's surface appeared distorted. Previous studies have found that the morphological distortion of the attached RBCs is related to compromised oxygen transport to the tissue, prevention tissue regeneration through re-epithelialization and angiogenesis and reduced inflammation in diabetic wounds.[73,74] The altered morphology of RBC shape can also increase blood viscosity, interrupt biomolecule transport to the wound site, compromise hemostatic properties, delay wound healing, *etc.*[75] The biconcave shape of the attached RBCs on the Gel/SA@PL hydrogel's surface contributes to

overcoming the transport obstacles of the required biomolecules for diabetic wound healing.

3.10 *In vitro* bacterial response study

Diabetic chronic wounds are more exposed to bacterial infection due to delayed healing with increased wound site exposure to microbes, diabetes induced ischemia, and angiopathy, which hinder oxygenation and increase the risk of infection. Hence, the antibacterial property of a wound dressing used for treating chronic wounds is an important parameter to be considered.[76] Fig. 6(c) illustrates complete inhibition of bacterial growth of both Gram-positive pathogenic bacteria, *S.aureus*, and Gram-negative pathogenic bacteria, *E.coli* on the hydrogels' as well as bacterial penetration through the hydrogel structure. On the other hand, gauze control depicted dense bacterial colony formation on the hydrogels surface and effective passage for bacterial penetration, confirming the bacterial protection barrier of the IPN structure of the hydrogels. Hyperglycemia in diabetes can induce strong biofilm formation by the microbes.[77] The presence of hydrophilic functional groups in gelatin and PL prevented the attachment and growth of hydrophobic *S.aureus* and *E.coli* on the hydrogel's surface. The dense three dimensional crosslinked IPN of Gel/SA with its small pores prevented the progression of the bacteria inside the structure.[78,79] The inhibition of bacterial growth on the hydrogel's surface and its penetration through the hydrogel makes Gel/SA@PL hydrogel a potential candidate for diabetic wound dressing. Gel/SA@PL as a hydrogel wound dressing can successfully prevent the contamination of the dressing and the risk of bacterial infection at the wound site.

3.11 *In vitro* PL release study

Drug release from the hydrogel occurs in two phases: (a) early rapid burst release and (b) extended diffusion controlled release. The initial phase occurs due to the presence of the drug at the hydrogel matrix surface and a higher drug concentration gradient across the matrix membrane. The final phase is controlled by the diffusion of the drug in the matrix and is comparatively slower than the initial phase due to the matrix dimension, which acts as a path for the drug in the hydrogel matrix.[80] PL release from Gel/SA@PL hydrogel was assessed using UV-Vis Spectrophotometry. Fig. 6(a) shows that Gel/

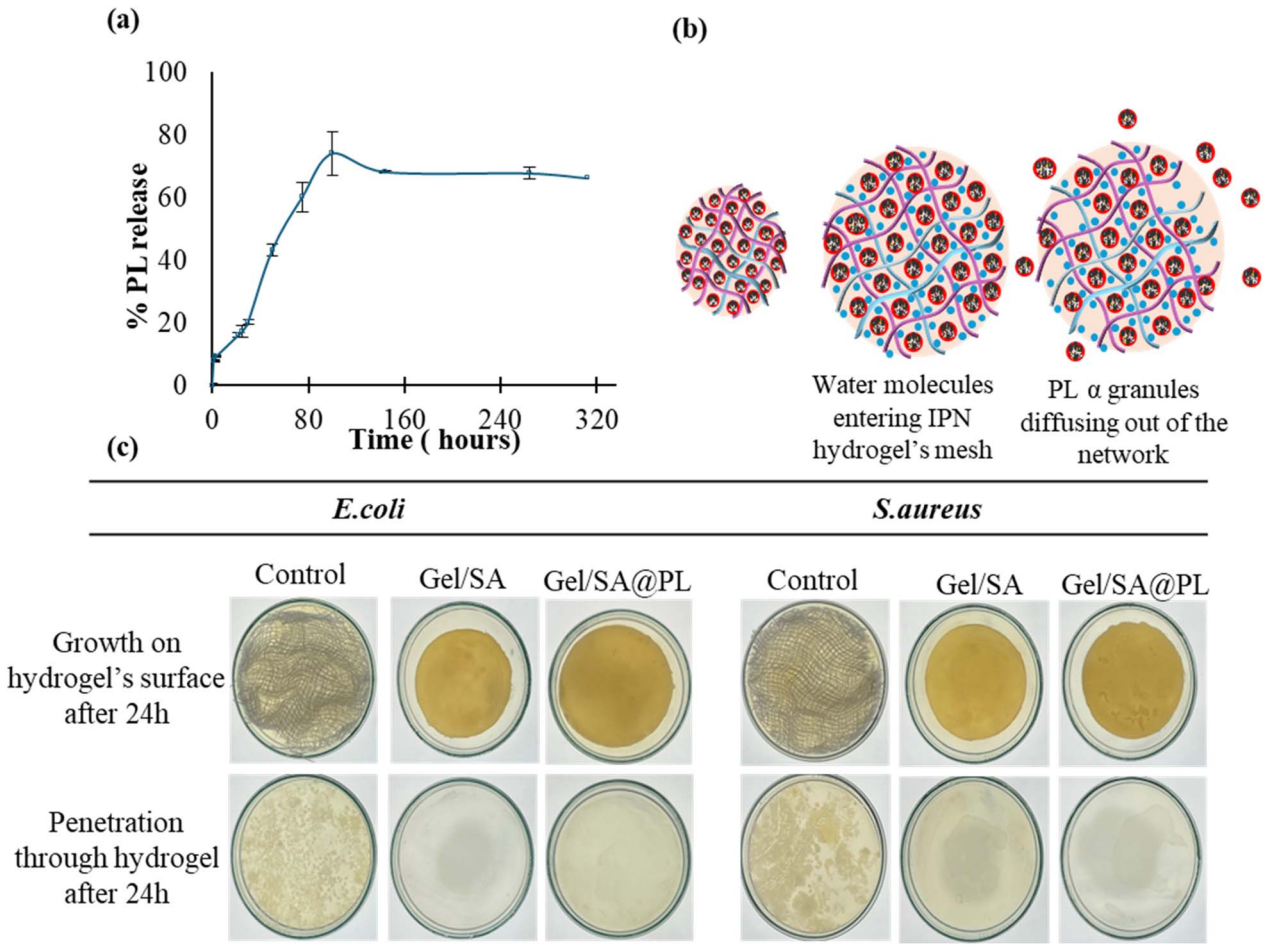

Fig. 6 PL release kinetics and antibacterial activity of the hydrogels. (a) PL release study of Gel/SA@PL hydrogel where entrapped PL biomolecules were released from the hydrogel over the 14 day period. (b) Fickian diffusion mechanism of PL biomolecules release from Gel/SA@PL hydrogel. (c) Bacterial growth on the hydrogel's surface and penetration through the hydrogel were analyzed for both *E. coli* and *S.aureus*. Both the hydrogels exhibited prevention of bacterial growth on their surfaces and their penetration.

Table 1 Drug release kinetics model fitting of PL. Korsmeyer–Peppas model with the highest R^2 value indicated the fiction diffusion mechanism of PL biomolecules released from the hydrogel

Zero order	First order	Korsmeyer–Peppas		Higuchi
R^2	R^2	R^2	n	R^2
0.3978	0.5109	**0.9267**	**0.392**	0.911

SA@PL hydrogel released 70% of PL in 14 days, offering sustained delivery aligned with wound healing timeline. Previous studies have demonstrated that gelatin based hydrogels have been able to release <70% of the drug in a prolonged period.[37] In this study, incorporation of sodium alginate as a secondary network provided enhanced controlled release of the PL growth factors in physiological conditions.[39]

The release data was analyzed by fitting in different drug release kinetics models, including zero order, first order, Korsmeyer–Peppas, Higuchi, *etc.* (Table 1). n value $\leq$ 0.45 indicates Fickian diffusion kinetics where the drug release is diffusion controlled as the solvent permeation into the hydrogel matrix is faster than the polymer chain disentanglements. 0.45 $\leq n \leq$ 0.89 indicates nonfickian diffusion kinetics, indicating diffusion and erosion controlled drug release. $n \geq$ 0.89 denotes Case II transport, where polymer disentanglement controls drug release at a constant rate.[81]

PL release from Gel/SA@PL hydrogel followed the Korsmeyer–Peppas model with the highest R^2 value and an n value of 0.39 < 0.45, indicating the Fickian diffusion mechanism, illustrated in Fig. 6(b). The release of PL from the hydrogel matrix is driven by matrix swelling and diffusion of growth factor molecules. The first phase of drug release occurs during the swelling of the hydrogel when a large amount of water enters the polymer network of the hydrogel matrix. The IPN structure of the Gel/SA@PL hydrogel limited solvent transport and polymer disentanglement, causing diffusion of the growth factors to become the dominant release factor.[38] The sustained manner of degradation of the IPN hydrogel over five days facilitated the slow diffusion of almost 70% of the PL biomolecules into the outer medium during the final phase of the drug release.

3.12 *In vivo* wound healing assessment

The wound healing dynamics were analyzed by H & E and MT staining of the tissues collected from a full thickness diabetic wound model. Type 2 diabetes was induced in Swiss albino mice by injecting multiple low doses of streptozotocin for five days, and the diabetic condition was confirmed by the blood glucose level after 15 days (Fig. 7(a)). The images of the control, Gel/SA hydrogel treated, and Gel/SA@PL hydrogel treated wound are displayed in Fig. 7(b), where the Gel/SA@PL hydrogel treated wound illustrated better wound healing than both the control and Gel/SA hydrogel treated wounds. After 14 days, the Gel/SA@PL hydrogel treated wound was almost fully closed with a minimal scar, whereas the control and Gel/SA hydrogel treated wounds were not fully healed. To verify the findings, wound areas were measured to analyze the wound closure rate, and it can be observed in Fig. 7(c) that Gel/SA@PL hydrogel closed 99.2% of the wound, which is significantly higher than the control wound's closure after 14 days. The growth factors of PL incorporated in Gel/SA@PL hydrogel played a significant role in wound contraction on days 3 and 7, which can be analyzed from the wound closure rate of Gel/SA hydrogel treated and Gel/SA@PL hydrogel treated wound on these days. After 3 and 7 days, Gel/SA@PL hydrogel treated wounds exhibited higher wound closure rates than Gel/SA hydrogel treated wounds. This wound closure rate is primarily governed by inflammation, proliferation, and tissue remodeling. The proliferation phase consists of three stages: (a) re-epithelialization, (b) angiogenesis, and (c) granulation tissue formation with a duration of 4–21 days.[82] H & E and MT staining of the wound tissues were analyzed to obtain deep insights into the tissue architecture in these phases of wound healing. The epithelial gap was visualized and measured from the H & E staining of the wound tissues after 3 days. In Fig. 7(d and e), it is seen that the epithelial gap was the lowest in Gel/SA@PL hydrogel treated wound tissue. Whereas the hydrogel treated wound tissues elicited a lower epithelial gap than the control wound tissue, PL growth factors incorporated Gel/SA@PL hydrogel treated wound tissue displayed a significantly lower epithelial gap than the Gel/SA hydrogel treated wound tissue after 3 days in Fig. 7(d). A lower epithelial gap indicates higher re-epithelialization, which forms the epidermal line at the damaged wound site with epithelial cells.[82] The migration of epithelial cells at the wound site is controlled by external factors, such as, optimal water content and internal factors, such as, growth factors and cytokines at the wound site.[60,83] The control diabetic wound exhibited the slowest re-epithelialization because chronic diabetic wound lacks both these factors due to hyperglycemia, which compromises the wound's re-epithelialization, causing impaired healing.[84] Gel/SA hydrogel treated wound site exhibited better re-epithelialization than the control with the formation of stratum corneum at the newly formed epithelial line due to the sodium alginate's property of maintaining the moisture content and gelatin's inherent tendency of promoting keratinocyte proliferation.[85] However, the most enhanced re-epithelialization was observed in Gel/SA@PL hydrogel treated wound tissue with the formation of both the stratum corneum and stratum spinosum at the newly formed epidermis than both control and Gel/SA hydrogel treated wounds due to its proper regulation of both the external and internal factors necessary for efficient wound healing on day 3. Gel/SA@PL hydrogel contains both sodium alginate and PL, where sodium alginate keeps the wound moist and makes the wound site favorable for the migration of epithelial cells stimulated by the release of HGF, KGF, and EGF from PL, facilitating the re-epithelialization.[70] Fig. 7(d) displays that the newly formed epidermis connected the epithelial gap after 7 days, and the blood vessels were formed to supply the intrinsic growth factors, cytokines, and nutrients to accelerate the healing. Angiogenesis was further confirmed by quantifying the newly formed blood vessels from the H & E staining of the wound tissues after 7 days. It can be observed in Fig. 7(f) that Gel/SA@PL hydrogel treated wound tissue showed significantly

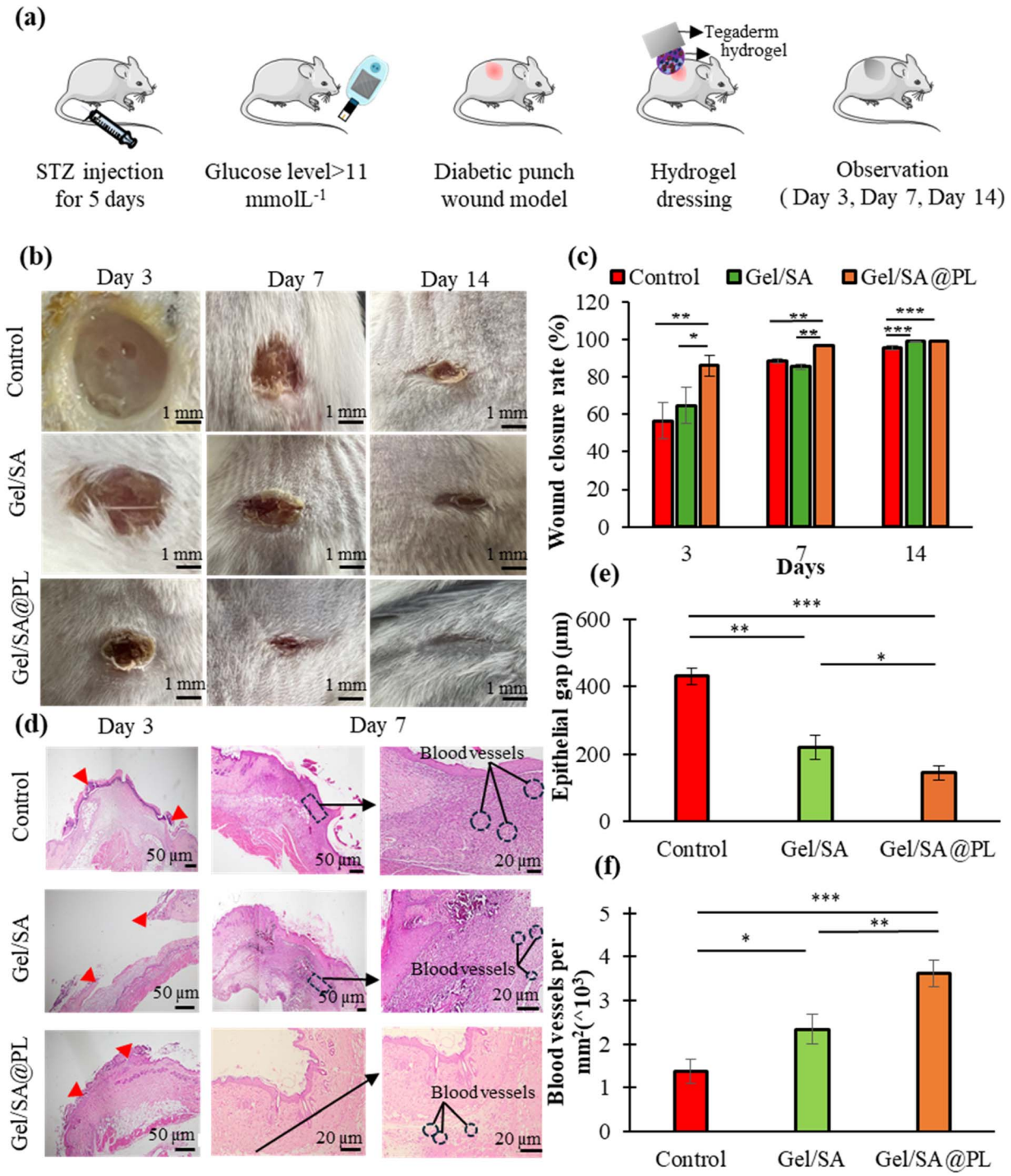

Fig. 7 (a) Diabetic wound model preparation in Swiss albino mice. (b and c) External images of control, Gel/SA hydrogel, and Gel/SA@PL hydrogel treated wounds and their wound closure rate on days 3, 7, and 14. (d) H & E staining of control, Gel/SA, and Gel/SA@PL hydrogel treated wounds on day 3 and day 7. (e) The epithelial gap of all wounds on day 3. The epithelial gap of Gel/SA@PL hydrogel treated wound was significantly lower than that of the Gel/SA hydrogel wound. (f) Quantification of blood vessels per area was measured from the H&E staining of control, Gel/SA, and Gel/SA@PL hydrogel treated wounds on day 7. Significantly higher blood vessels per area were found in Gel/SA@PL hydrogel treated wounds compared to other wounds after 7 days. Significance is denoted by *($P < 0.05$), **($P < 0.01$), ***($P < 0.001$).

higher angiogenesis than both the control and Gel/SA hydrogel treated wound tissues. ECM protein, collagen derived gelatin, in Gel/SA IPN has an arginine-glycine-aspartic acid RGD peptide sequence acting as a cell attachment site, which triggers endothelial cell adhesion, promoting angiogenesis.[86,87] This characteristic of Gel/SA hydrogel triggered angiogenesis and showed more blood vessels than the control wound tissue. However, PL associated growth factors, TGF(α-β), VEGF, EGF, CTGF, HGF, Ang-1, SDF-1α, and TNF entrapped in Gel/SA@PL hydrogel facilitated by the cell attachment sites of gelatin in

the IPN played an active role in endothelial cell differentiation, mitogenesis, and proliferation to form the highest number of blood vessels at the wound site and established enhanced vessel permeability to provide sufficient nutrients and oxygen to the wound site.[83]

The progression of re-epithelialization was further analyzed by visualizing and measuring the epithelial thickness from the H & E staining of the wound tissues on days 7 and 14. Fig. 8(a) reveals that the epithelial thickness reduced after 7 days in all the samples, triggering the development of healthy epidermal tissue structure. It can be observed in Fig. 8(b) that the epithelial thickness was the lowest in Gel/SA@PL hydrogel treated wound tissue due to the early initiation of the development of epidermis with stratum corneum formation on day 3. The high proliferation of epithelial cells caused this phenomenon, which was triggered by the PL associated growth factors released from the hydrogel.

Inflammatory cells were measured from the H & E staining of the wound tissues after 7 and 14 days to analyze the pattern of chronic inflammation in the diabetic wound. After 7 and 14 days, hydrogel treated wound tissues exhibited a lower number of inflammatory cells than the control wound tissue in Fig. 8(c). In diabetic chronic wounds, the wound is generally confined in a chronic inflammation loop, which prohibits its progression to the proliferation and remodeling phase.[1] The inflammation persisted in both the control and Gel/SA hydrogel treated wound tissue, as there were no significant differences between the number of inflammatory cells on days 7 and 14. However, Gel/SA@PL hydrogel treated wound tissue elicited a significantly lower number of inflammatory cells on day 14 than on day 7, indicating the prevention of chronic inflammation and progression of the wound healing dynamics towards proliferation. The release of PL from Gel/SA@PL hydrogel provided biomolecules, epidermal growth factor (EGF), FGF, cytokine, and TNF.[83] These biomolecules enhanced fibroblast proliferation and produced fibroblasts, which migrated to the wound area in response to FGF and TGF and released MMP inhibitors, preventing the high protease and MMP activity. Reduced expression of MMPs and proteases in the chronic wound decreased the number of inflammatory cells preventing chronic inflammation.[88,89]

The H&E staining of the Ge/SA@PL hydrogel treated wound tissues expressed the presence of adipocytes in the dermal layer of the wound area on all days, as shown in Fig. 9(a). However, the dermal adipocytes were not present in the control and the Gel/SA hydrogel treated wounds. The quantification of the adipocytes from the H&E staining of Gel/SA@PL hydrogel treated wound tissue revealed that the number of adipocytes significantly reduced with time. Granulation tissue is a structural framework of connective tissue rich in fibroblasts and newly formed blood vessels, providing nutrients to the wound site and protection from bacteria from the death cells by destroying them.[90] Adipocyte rich granulation tissue formation can be triggered by differentiation and proliferation of adipose derived stem cells, dermal fibroblast, and endothelial cells to form ECM of this tissue.[82,91] PL biomolecules in the Gel/SA@PL hydrogel stimulated adipose derived stem cell differentiation from mesenchymal stem cells (MSC) and favored its

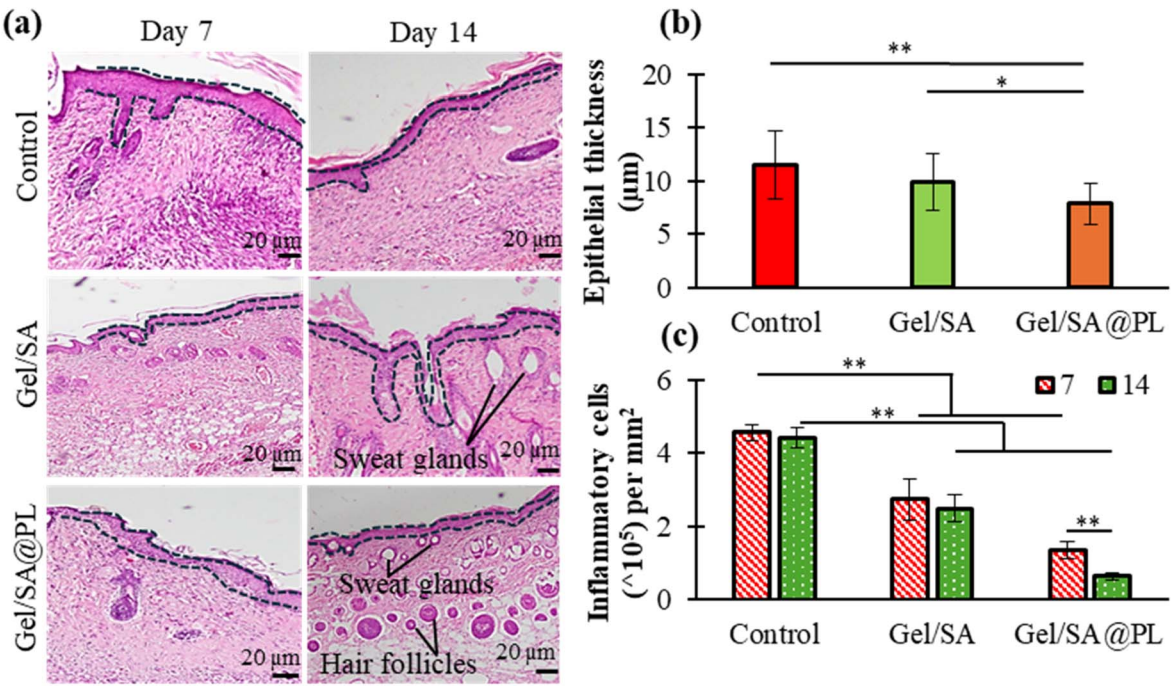

Fig. 8 (a) H & E staining of control, Gel/SA, and Gel/SA@PL hydrogel treated wounds for epithelial membrane thickness visualization. (b) Epithelial thickness measurement of all the wounds on day 14. After 14 days, thickness reduced significantly in the Gel/SA@PL hydrogel treated wound. (c) Number of inflammatory cells on the control, Gel/SA hydrogel treated, and Gel/SA@PL hydrogel treated wounds on days 7 and 14. The significantly lower number of inflammatory cells at the Gel/SA@PL hydrogel treated wound on day 14 than on day 7 indicated successful prevention of chronic inflammation at the diabetic wound. Significance is denoted by *($P < 0.05$), **($P < 0.01$), ***($P < 0.001$).

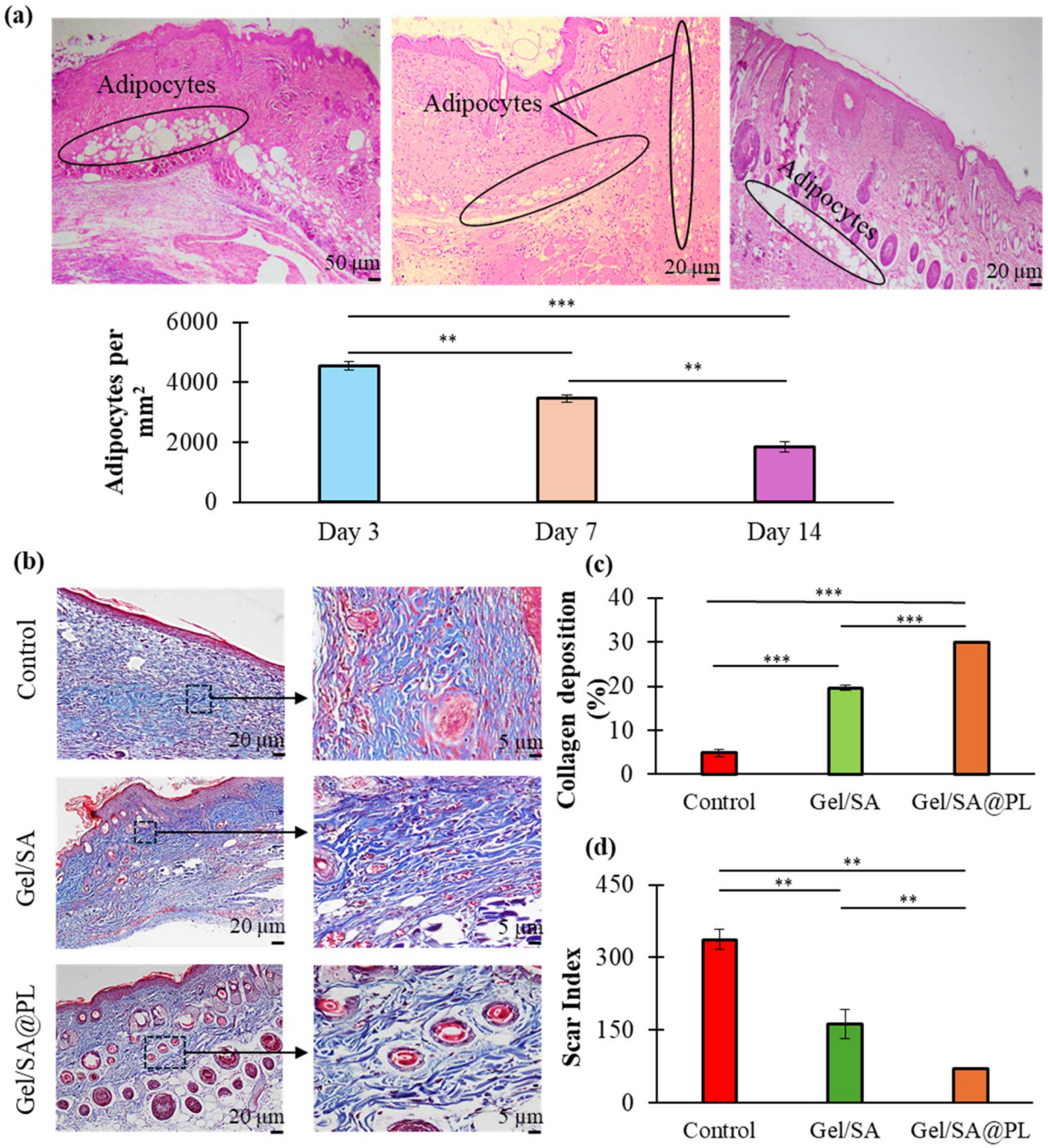

Fig. 9 (a) The number of adipocytes accumulated on the Gel/SA@PL hydrogel treated wound sites on days 3, 7, and 14. The significant reduction in the number of adipocytes per area in 11 days coincided with the granulation tissue formation period in normal wound healing. (b) MT staining of the control, Gel/SA, and Gel/SA@PL hydrogel treated wounds on day 14 for collagen structure analysis. (c) Collagen deposition percentage analysis of all the wounds on day 14. Gel/SA@PL hydrogel treated wound restored basketweave collagen structure with significantly higher collagen deposition than other wounds (d) Scar index of the control, Gel/SA hydrogeltreated, and Gel/SA@PL hydrogel treated wounds on day 14. The lowest scar index of the Gel/SA@PL hydrogel treated wound denoted a lower tendency of scar formation. Significance is denoted by *(P < 0.05), **(P < 0.01), ***(P < 0.001).

proliferation by preventing apoptosis of adipocyte precursor cells.[92,93] Adipocytes are highest on day 3 and lowest on day 14, which indicates that the granulation tissue formation initiated on day 3 and lasted for 14 days. The burst release of PL growth factors on day 3 accelerated adipose derived stem cell activity at the wound site with the highest number of adipocyte formation, which engendered granulation tissue formation. Increased adipocyte formation can attenuate the expression of α-smooth muscle actin (α-SMA) of human keloid fibroblasts and trigger collagen rearrangement.[94] On the other hand, the absence of such activity in the control and the Gel/SA hydrogel treated

wounds indicate delayed granulation tissue formation in these wounds.

Collagen structures of the wound tissues were analyzed from the MT staining of the tissues after 14 days, as shown in Fig. 9(b). Among all the wound tissues, the basketweave collagen structure governed the wound area of the Gel/SA@PL hydrogel treated wound tissue. This was further confirmed by the measurement of collagen deposition at the wound area of all the wound tissues from MT staining. Fig. 9(c) shows that MT staining expressed 45% basketweave pattern collagen deposition at the Gel/SA@PL hydrogel treated wound tissue, which was significantly higher than both the control and the Gel/SA hydrogel treated wound tissues on day 14 due to the negative regulation of α-SMA triggered by high adipose derived stem cell activity on day 3 and the release of growth factors, PDGF and TGF (α-β) by PL at the wound site. PDGF and TGF (α-β) play an important role in collagen synthesis and deposition at the wound site, leading to the restoration of healthy skin tissue structure at the wound site.[83] Gel/SA hydrogel treated wound had higher uniform collagen deposition than the control wound due to the natural ECM resembling the structure of the Gel/SA hydrogel, which favored collagen deposition.[95] Gel/SA@PL hydrogel treated wound tissue exhibited the lowest scar index compared to all the other wound tissues in Fig. 9(d). The Gel/SA@PL hydrogel yielded well organized collagen fiber accumulation at the wound site by day 14, resulting in skin appendage appearance and effectively preventing scar formation, as depicted in Fig. 8(a) and 7(b).[96]

Hair follicles at the wound site indicate the initiation of tissue remodeling because they are excellent mediator for triggering intrinsic signals for skin regeneration.[97] Platelets in PL released from the Gel/SA@PL hydrogel effectively stimulated hair follicle regeneration by activating hair follicle stem cells, reducing the probability of scar development at the wound site.[98]

Overall, the H & E and MT staining of the Gel/SA@PL hydrogel treated wound tissues illustrated reduced expression of inflammatory cells, enhanced re-epithelialization rate, angiogenesis, early initiation of granulation tissue formation with large number of adipocyte formation, and tissue remodeling with low scar index and established its efficacy in the restoration of natural wound healing dynamics with minimal scarring in diabetic wound successfully.

4 Conclusion

This study synthesized a novel pure natural polymer based hydrogel with an IPN to incorporate multiple growth factors rich PL. ATR-FTIR confirmed the formation of the IPN of gelatin and sodium alginate and its efficient incorporation of PL. Hydrophilic functional groups at the hydrogel's surface and its IPN associated small pores prevented bacterial contamination of both the hydrogels and reduced bacterial infection risk by preventing bacterial penetration through the hydrogel. PL was successfully loaded in the Gel/SA@PL hydrogel, and it provided a controlled release of 70% of its loaded PL in a pH seven simulated medium for 14 days, facilitated by its tuned degradation. This controlled release offered efficient delivery of PL associated biomolecules to the wound, battling the growth factor compromised healing of chronic diabetic wounds. The controlled delivery of the growth factor, CTGF, by the Gel/SA@PL hydrogel provided successful platelet adhesion during hemostasis and vastly improved the blood clotting rate. PL associated growth factors and cytokines delivered by the Gel/SA@PL hydrogel downregulated MMP activity and reduced the inflammatory cell expression at the wound site. The early termination of the inflammation phase accelerated re-epithelialization of the proliferation phase. The proliferation phase governed the wound site with angiogenesis and adipocyte expression to initiate granulation tissue formation and collagen rearrangement. High adipose derived stem cell activity triggered collagen rearrangement and accumulated 45% basketweave collagen structure at the wound site. Uniform reorganization of basketweave collagen structure expedited skin regeneration with a large number of hair follicles and sweat glands and inhibited scar development. These findings posited the idea that multiple natural polymer based Gel/SA@PL IPN hydrogel could efficiently entrap the biomolecules of PL and restore normal wound healing dynamics in chronic diabetic wounds by preventing bacterial infection risks, triggering high hemostatic activity, inhibiting the chronic inflammation loop, and enhancing proliferation and tissue modeling. Gel/SA@PL revived the natural wound healing phenomena in chronic diabetic wounds, leading to effective healing with reduced scar formation. The occurrence of natural wound healing stages in the required time frame confirmed the successful controlled delivery of PL to the wound site with sustained efficacy by the synthesized IPN hydrogel based delivery system.

Conflicts of interest

There are no conflicts to declare.

Data availability

The data supporting this article have been included in the manuscript.

Acknowledgements

The research project was funded by Research and Innovation in Science and Engineering (RISE), Bangladesh University of Engineering and Technology (BUET).

References

1 J. L. Burgess, W. A. Wyant, B. A. Abujamra, R. S. Kirsner and I. Jozic, *Diabetic Wound-Healing Science*, MDPI, 2021, DOI: 10.3390/medicina57101072.

2 O. Catanzano, F. Quaglia and J. S. Boateng, Wound dressings as growth factor delivery platforms for chronic wound healing, *Expert Opin. Drug Deliv.*, 2021, **18**(6), 737–759, DOI: 10.1080/17425247.2021.1867096.

3 M. A. Tibatan, D. Katana and C. M. Yin, The emerging role of nanoscaffolds in chronic diabetic wound healing: a new horizon for advanced therapeutics, *J. Biomater. Sci., Polym. Ed.*, 2025, **36**, 513–544, DOI: 10.1080/09205063.2024.2402148.
4 M. J. Martinez-Zapata, *et al.*, Autologous platelet-rich plasma for treating chronic wounds, *Cochrane Database Syst. Rev.*, 2016, **2016**(5), CD006899, DOI: 10.1002/14651858.CD006899.pub3.
5 T. del Pino-Sedeño, *et al.*, Platelet-rich plasma for the treatment of diabetic foot ulcers: A meta-analysis, *Wound Repair Regen.*, 2019, **27**(2), 170–182, DOI: 10.1111/wrr.12690.
6 R. Alves and R. Grimalt, A Review of Platelet-Rich Plasma: History, Biology, Mechanism of Action, and Classification, *Skin Appendage Disorders*, 2018, 18–24, DOI: 10.1159/000477353.
7 M. Nadra, W. Niu, M. Kurisawa, D. Rousson and M. Spector, Platelet-Rich Plasma Lysate-Incorporating Gelatin Hydrogel as a Scaffold for Bone Reconstruction, *Bioengineering*, 2022, **9**(10), 513, DOI: 10.3390/bioengineering9100513.
8 M. J. Martinez-Zapata, *et al.*, Autologous platelet-rich plasma for treating chronic wounds, *Cochrane Database Syst. Rev.*, 2012, **10**, CD006899, DOI: 10.1002/14651858.CD006899.PUB2.
9 H. A. Farghali, N. A. AbdElKader, M. S. Khattab and H. O. AbuBakr, Evaluation of subcutaneous infiltration of autologous platelet-rich plasma on skin-wound healing in dogs, *Biosci. Rep.*, 2017, **37**(2), BSR20160503, DOI: 10.1042/BSR20160503.
10 P. Losi, T. Al Kayal, M. Buscemi, I. Foffa, A. Cavallo and G. Soldani, Bilayered fibrin-based electrospun-sprayed scaffold loaded with platelet lysate enhances wound healing in a diabetic mouse model, *Nanomaterials*, 2020, **10**(11), 1–11, DOI: 10.3390/nano10112128.
11 S.-Y. Zheng, *et al.*, Therapeutic role of growth factors in treating diabetic wound, *World J. Diabetes*, 2023, **14**(4), 364–395, DOI: 10.4239/wjd.v14.i4.364.
12 J. Duarte, F. Mascarenhas-Melo, P. C. Pires, F. Veiga and A. C. Paiva-Santos, Multifunctional hydrogels-based therapies for chronic diabetic wound healing, *Eur. Polym. J.*, 2024, 113026, DOI: 10.1016/j.eurpolymj.2024.113026.
13 J. M. Dodda, K. Deshmukh, D. Bezuidenhout and Y.-C. Yeh, Hydrogels: Definition, History, Classifications, Formation, Constitutive Characteristics, and Applications, [Online], available: https://www.rsc.org.
14 Y. Zhao, Y. Wang, C. Niu, L. Zhang, G. Li and Y. Yang, Construction of polyacrylamide/graphene oxide/gelatin/sodium alginate composite hydrogel with bioactivity for promoting Schwann cells growth, *J. Biomed. Mater. Res., Part A*, 2018, **106**(7), 1951–1964, DOI: 10.1002/jbm.a.36393.
15 T. Nii, Strategies using gelatin microparticles for regenerative therapy and drug screening applications, *Molecules*, 2021, 6795, DOI: 10.3390/molecules26226795.
16 T. U. Rashid and *et al.*, *Gelatin-Based Hydrogels*, 2019, pp. 1601–1641, DOI: 10.1007/978-3-319-77830-3_53.
17 V. Manish, A. Arockiarajan and G. Tamadapu, Influence of water content on the mechanical behavior of gelatin based hydrogels: Synthesis, characterization, and modeling, *Int. J. Solids Struct.*, 2021, **233**, 111219, DOI: 10.1016/j.ijsolstr.2021.111219.
18 S. Jeong, B. Kim, H.-C. Lau and A. Kim, Pharmaceutics Gelatin-Alginate Complexes for EGF Encapsulation: Effects of H-Bonding and Electrostatic Interactions, *Pharmaceutics*, 2019, 530, DOI: 10.3390/pharmaceutics11100530.
19 L. Wang, *et al.*, A Physically Cross-Linked Sodium Alginate-Gelatin Hydrogel with High Mechanical Strength, *ACS Appl. Polym. Mater.*, 2021, **3**(6), 3197–3205, DOI: 10.1021/acsapm.1c00404.
20 M. Bahadoran, A. Shamloo and Y. D. Nokoorani, Development of a polyvinyl alcohol/sodium alginate hydrogel-based scaffold incorporating bFGF-encapsulated microspheres for accelerated wound healing, *Sci. Rep.*, 2020, **10**(1), 7–9, DOI: 10.1038/s41598-020-64480-9.
21 A. R. Abbasi, *et al.*, Bioinspired sodium alginate based thermosensitive hydrogel membranes for accelerated wound healing, *Int. J. Biol. Macromol.*, 2020, **155**, 751–765, DOI: 10.1016/j.ijbiomac.2020.03.248.
22 Y. M. Kolambkar, *et al.*, An alginate-based hybrid system for growth factor delivery in the functional repair of large bone defects, *Biomaterials*, 2011, **32**(1), 65–74, DOI: 10.1016/j.biomaterials.2010.08.074.
23 T. Jiao, R. Zhou, J. Jiao, J. Jiao and Q. Lian, Extrusion/Inkjet Printing of Verteporfin-Loaded Bilayer Skin Substitutes for Wound Healing and Structure Reconstruction, *J. Bionic Eng.*, 2024, **21**(6), 2969–2984, DOI: 10.1007/S42235-024-00585-5/METRICS.
24 J. Zhou, M. Li and Y. Hui, Hemostatic sponge based on easily prepared crosslinked gelatin and sodium alginate for wound healing, *J. Mater. Sci.*, 2024, **59**, 8408–8426.
25 M. A. Amini, I. Khodadadi, H. Tavilani, R. Abbasalipourkabir, M. Azizi, K. Rashidi, H. Samadian and J. Karimi, Fabrication, characterization, and application of gelatin/alginate-based hydrogels incorporating selenium-doped deferoxamine-derived carbon quantum dots: In vitro and in vivo studies, *Int. J. Biol. Macromol.*, 2025, 140569.
26 M. M. Babić Radić, *et al.*, Development of Nano ZnO-Embedded Gelatin/Alginate Bioscaffolds for Potential Skin Tissue Regeneration via Oxidative Stress Modulation and ECM Mimicry, *Biopolymers*, 2025, **116**(5), e70046, DOI: 10.1002/bip.70046.
27 R. Zhang, X. Liu, W. Zhang, B. Cui, Y. Du, Y. Huang, W. Li, Q. Liu, C. Ren and Z. Tang, A review of polysaccharide-based hydrogels: From structural modification to biomedical applications, *Int. J. Biol. Macromol.*, 2025, 143519.
28 Q. Chen, X. Tian, J. Fan, H. Tong, Q. Ao and X. Wang, An interpenetrating alginate/gelatin network for three-dimensional (3D) cell cultures and organ bioprinting, *Molecules*, 2020, **25**(3), 756, DOI: 10.3390/molecules25030756.
29 X. Hou, *et al.*, Sodium alginate-type B gelatin double-network hydrogels: the dual actions of ionic crosslinking and the salting-out effect, *Int. J. Biol. Macromol.*, 2025, **338**, 149743.

30 L. Yuan, Y. Wu, Q. sheng Gu, H. El-Hamshary, M. El-Newehy and X. Mo, Injectable photo crosslinked enhanced double-network hydrogels from modified sodium alginate and gelatin, *Int. J. Biol. Macromol.*, 2017, **96**, 569–577, DOI: 10.1016/j.ijbiomac.2016.12.058.

31 J. Skopinska-Wisniewska, M. Tuszynska and E. Olewnik-Kruszkowska, Comparative study of gelatin hydrogels modified by various cross-linking agents, *Materials*, 2021, **14**(2), 1–17, DOI: 10.3390/ma14020396.

32 E. S. Dragan, Design and applications of interpenetrating polymer network hydrogels. A review, *Chem. Eng. J.*, 2014, 572–590, DOI: 10.1016/j.cej.2014.01.065.

33 M. S. Silverstein, Interpenetrating polymer networks: So happy together?, *Polymer*, 2020, **207**, 122929, DOI: 10.1016/j.polymer.2020.122929.

34 X. Zhang, *et al.*, Berberine carried gelatin/sodium alginate hydrogels with antibacterial and EDTA-induced detachment performances, *Int. J. Biol. Macromol.*, 2021, **181**, 1039–1046, DOI: 10.1016/j.ijbiomac.2021.04.114.

35 L. Wang, *et al.*, A Physically Cross-Linked Sodium Alginate-Gelatin Hydrogel with High Mechanical Strength, *ACS Appl. Polym. Mater.*, 2021, **3**(6), 3197–3205, DOI: 10.1021/acsapm.1c00404.

36 X. Zhang, *et al.*, Engineering Platelet-Rich Plasma Based Dual-Network Hydrogel as a Bioactive Wound Dressing with Potential Clinical Translational Value, *Adv. Funct. Mater.*, 2021, **31**(8), 1–14, DOI: 10.1002/adfm.202009258.

37 C. Kaliampakou, N. Lagopati, E. A. Pavlatou and C. A. Charitidis, Alginate–Gelatin Hydrogel Scaffolds; An Optimization of Post-Printing Treatment for Enhanced Degradation and Swelling Behavior, *Gels*, 2023, **9**(11), 857, DOI: 10.3390/gels9110857.

38 A. P. Dhand, J. H. Galarraga and J. A. Burdick, Enhancing Biopolymer Hydrogel Functionality through Interpenetrating Networks, *Trends Biotechnol.*, 2021, 519–538, DOI: 10.1016/j.tibtech.2020.08.007.

39 Z. Zou, *et al.*, A sodium alginate-based sustained-release IPN hydrogel and its applications, *RSC Adv.*, 2020, 39722–39730, DOI: 10.1039/d0ra04316h.

40 E. Van Den Bosch and C. Gielens, Gelatin degradation at elevated temperature, *Int. J. Biol. Macromol.*, 2003, **32**(3–5), 129–138, DOI: 10.1016/S0141-8130(03)00046-1.

41 S. O. Firdous, K. Arif Siew, Y. Wong, Xu Li, and M. T. Arafat, In situ crosslinked electrospun gelatin matrix with unoxidized tannic acid through stable hydrogen bonding.

42 K. Terao, *et al.*, Reagent-free crosslinking of aqueous gelatin: Manufacture and characteristics of gelatin gels irradiated with gamma-ray and electron beam, *J. Biomater. Sci. Polym. Ed.*, 2003, **14**(11), 1197–1208, DOI: 10.1163/156856203322553437.

43 M. T. Arafat, M. M. Mahmud, S. Y. Wong and X. Li, PVA/PAA based electrospun nanofibers with pH-responsive color change using bromothymol blue and on-demand ciprofloxacin release properties, *J. Drug Deliv. Sci. Technol.*, 2021, **61**, 102297, DOI: 10.1016/j.jddst.2020.102297.

44 K. Kobra, S. Y. Wong, M. A. J. Mazumder, X. Li and M. T. Arafat, Xanthan and gum acacia modified olive oil based nanoemulsion as a controlled delivery vehicle for topical formulations, *Int. J. Biol. Macromol.*, 2023, **253**, 126868, DOI: 10.1016/J.IJBIOMAC.2023.126868.

45 N. Datta, *et al.*, Self-assembled sodium alginate polymannuronate nanoparticles for synergistic treatment of ophthalmic infection and inflammation: Preparation optimization and in vitro/vivo evaluation, *Int. J. Biol. Macromol.*, 2024, **262**, 130038, DOI: 10.1016/J.IJBIOMAC.2024.130038.

46 L. H. Tithy, A. Rahman, S. Y. Wong, X. Li and M. T. Arafat, Chitosan/starch based unoxidized tannic acid modified microparticles for rapid hemostasis with broad spectrum antibacterial activity, *Carbohydr. Polym.*, 2024, **336**, 122111, DOI: 10.1016/J.CARBPOL.2024.122111.

47 F. Yañez, J. L. Gomez-Amoza, B. Magariños, A. Concheiro and C. Alvarez-Lorenzo, Hydrogels porosity and bacteria penetration: Where is the pore size threshold?, *J. Memb. Sci.*, 2010, **365**(1–2), 248–255, DOI: 10.1016/j.memsci.2010.09.012.

48 S. A. Bernal-Cháveza, S. Alcalá-Alcaláb, D. Cerecedoc and A. Ganem-Ronderoa, *Eur. J. Pharm. Sci.*, 2020, **146**, 105231.

49 B. L. Furman, Streptozotocin-Induced Diabetic Models in Mice and Rats, *Curr. Protoc. Pharmacol.*, 2015, **70**(1), 47, DOI: 10.1002/0471141755.ph0547s70.

50 T. Hasan Aneem, *et al.*, Antimicrobial peptide immobilization on catechol-functionalized PCL/alginate wet-spun fibers to combat surgical site infection, *J. Mater. Chem. B*, 2024, **12**(30), 7401–7419, DOI: 10.1039/d4tb00889h.

51 N. Nakajima and Y. Ikada, Mechanism of Amide Formation by Carbodiimide for Bioconjugation in Aqueous Media, 1995, [Online], available: https://pubs.acs.org/sharingguidelines.

52 Z. Zhou, *et al.*, Fabrication and physical properties of gelatin/sodium alginate/hyaluronic acid composite wound dressing hydrogel, *J. Macromol. Sci., Part A: Pure Appl. Chem.*, 2014, **51**(4), 318–325, DOI: 10.1080/10601325.2014.882693.

53 J. Babrnáková, *et al.*, Synergistic effect of bovine platelet lysate and various polysaccharides on the biological properties of collagen-based scaffolds for tissue engineering: Scaffold preparation, chemo-physical characterization, in vitro and ex ovo evaluation, *Mater. Sci. Eng., C*, 2019, **100**, 236–246, DOI: 10.1016/j.msec.2019.02.092.

54 S. Afzal, *et al.*, The structural, crystallinity, and thermal properties of pH-responsive interpenetrating gelatin/sodium alginate-based polymeric composites for the controlled delivery of cetirizine HCl, *Turk. J. Pharm. Sci.*, 2018, **15**(1), 63–76, DOI: 10.4274/tjps.64326.

55 V. Gounden and M. Singh, Hydrogels and Wound Healing: Current and Future Prospects, *Gels*, 2024, 43, DOI: 10.3390/gels10010043.

56 K. Bialik-Wąs, K. Pluta, D. Malina, M. Barczewski, K. Malarz and A. Mrozek-Wilczkiewicz, Advanced SA/PVA-based hydrogel matrices with prolonged release of Aloe vera as promising wound dressings, *Mater. Sci. Eng., C*, 2021, **120**, 111667, DOI: 10.1016/j.msec.2020.111667.

57 I. Van Nieuwenhove, *et al.*, Gelatin- and starch-based hydrogels. Part A: Hydrogel development, characterization and coating, *Carbohydr. Polym.*, 2016, **152**, 129–139, DOI: 10.1016/j.carbpol.2016.06.098.

58 H. Hossainpour, *et al.*, Gelatin-sodium alginate hydrogel infused with Onosma dichroanthum Boiss. root extract: Preparation, characterization, and application in wound dressing, *Biochem. Biophys. Rep.*, 2025, **44**, 102236, DOI: 10.1016/j.bbrep.2025.102236.

59 G. J. Martínez-Díaz, D. Nelson, W. C. Crone and W. J. Kao, Mechanical and Chemical Analysis of Gelatin-Based Hydrogel Degradation, *Macromol. Chem. Phys.*, 2003, **204**(15), 1898–1908, DOI: 10.1002/macp.200350042.

60 R. Xu, *et al.*, Controlled water vapor transmission rate promotes wound-healing via wound re-epithelialization and contraction enhancement, *Sci. Rep.*, 2016, **6**, 24596, DOI: 10.1038/srep24596.

61 Z. Zhou, *et al.*, Fabrication and physical properties of gelatin/sodium alginate/hyaluronic acid composite wound dressing hydrogel, *J. Macromol. Sci., Part A: Pure Appl. Chem.*, 2014, **51**(4), 318–325, DOI: 10.1080/10601325.2014.882693.

62 B. Balakrishnan, M. Mohanty, P. R. Umashankar and A. Jayakrishnan, Evaluation of an in situ forming hydrogel wound dressing based on oxidized alginate and gelatin, *Biomaterials*, 2005, **26**(32), 6335–6342, DOI: 10.1016/j.biomaterials.2005.04.012.

63 K. Klimek and G. Ginalska, Proteins and peptides as important modifiers of the polymer scaffolds for tissue engineering applications-A review, *Polymers*, 2020, 844, DOI: 10.3390/POLYM12040844.

64 L. Liu, A. Chakma and X. Feng, Gas permeation through water-swollen hydrogel membranes, *J. Memb. Sci.*, 2008, **310**(1–2), 66–75, DOI: 10.1016/j.memsci.2007.10.032.

65 F. Wang, *et al.*, Constructing rapid water vapor transport channels within mixed matrix membranes based on two-dimensional mesoporous nanosheets, *Commun. Chem.*, 2022, **5**(1), 65, DOI: 10.1038/s42004-022-00681-9.

66 Y. Zhao, L. Ma, R. Zeng, M. Tu and J. Zhao, Preparation, characterization and protein sorption of photo-crosslinked cell membrane-mimicking chitosan-based hydrogels, *Carbohydr. Polym.*, 2016, **151**, 237–244, DOI: 10.1016/j.carbpol.2016.05.067.

67 R. Fitridge and M. Thompson, Mechanisms of Vascular Disease, *Mechanisms of Vascular Disease: A Reference Book for Vascular Specialists*, 2011, accessed: Feb. 16, 2025, [Online]. available: https://www.ncbi.nlm.nih.gov/books/NBK534260/.

68 A. I. Vinik, T. Erbas, T. Sun Park, R. Nolan and G. L. Pittenger, Platelet Dysfunction in Type 2 Diabetes, *Diabetes Care*, 2001, **24**(8), 1476–1485, DOI: 10.2337/DIACARE.24.8.1476.

69 Y. Huang, *et al.*, Degradable Gelatin-Based IPN Cryogel Hemostat for Rapidly Stopping Deep Noncompressible Hemorrhage and Simultaneously Improving Wound Healing, *Chem. Mater.*, 2020, **32**(15), 6595–6610, DOI: 10.1021/acs.chemmater.0c02030.

70 P. Everts, K. Onishi, P. Jayaram, J. F. Lana and K. Mautner, Platelet-rich plasma: New performance understandings and therapeutic considerations in 2020, *Int. J. Mol. Sci.*, 2020, 1–36, DOI: 10.3390/ijms21207794.

71 I. Cicha, C. D. Garlichs, W. G. Daniel and M. Goppelt-Struebe, Activated human platelets release connective tissue growth factor, *Thromb. Haemost.*, 2004, **91**(4), 755–760, DOI: 10.1160/TH03-09-0602.

72 W. Liang, *et al.*, A multifunctional green antibacterial rapid hemostasis composite wound dressing for wound healing, *Biomater. Sci.*, 2021, **9**(21), 7124–7133, DOI: 10.1039/d1bm01185e.

73 Red Blood Cell (RBC) Morphology: Description and Causes, accessed: Jun. 10, 2024, [Online], available: https://myhematology.com/red-blood-cells/red-blood-cell-rbc-morphology/.

74 Y. A. GUAN, *et al.*, Sustained oxygenation accelerates diabetic wound healing by promoting epithelialization and angiogenesis and decreasing inflammation, *Sci. Adv.*, 2021, **7**(35), eabj0153.

75 J. R. Byrnes and A. S. Wolberg, Blood Spotlight Red blood cells in thrombosis, *Blood*, 2017, 1795–1799, DOI: 10.1182/blood-2017-03.

76 S. Abri, *et al.*, Chitosan-based multifunctional oxygenating antibiotic hydrogel dressings for managing chronic infection in diabetic wounds, *Biomater. Sci.*, 2024, 3458–3470, DOI: 10.1039/d4bm00355a.

77 J. L. Burgess, W. A. Wyant, B. A. Abujamra, R. S. Kirsner and I. Jozic, Diabetic wound-healing science, *Medicina*, 2021, 1072, DOI: 10.3390/medicina57101072.

78 F. Yañez, J. L. Gomez-Amoza, B. Magariños, A. Concheiro and C. Alvarez-Lorenzo, Hydrogels porosity and bacteria penetration: Where is the pore size threshold?, *J. Memb. Sci.*, 2010, **365**(1–2), 248–255, DOI: 10.1016/j.memsci.2010.09.012.

79 G. M. Bruinsma, H. C. Van Der Mei and H. J. Busscher, Bacterial adhesion to surface hydrophilic and hydrophobic contact lenses, *Biomaterials*, 2001, **22**(24), 3217–3224, DOI: 10.1016/S0142-9612(01)00159-4.

80 Y. Fu and W. J. Kao, Drug release kinetics and transport mechanisms of non-degradable and degradable polymeric delivery systems, *Expert Opin. Drug Delivery*, 2010, 429–444, DOI: 10.1517/17425241003602259.

81 H. Baishya, Application of Mathematical Models in Drug Release Kinetics of Carbidopa and Levodopa ER Tablets, *J. Drug Dev.*, 2017, **06**(02), 1–8, DOI: 10.4172/2329-6631.1000171.

82 M. El Mohtadi, K. Whitehead, N. Dempsey-Hibbert, A. Belboul and J. Ashworth, Estrogen deficiency – a central paradigm in age-related impaired healing?, Leibniz Research Centre for Working Environment and Human Factors, *EXCLI J.*, 2021, 99–116, DOI: 10.17179/excli2020-3210.

83 P. Everts, K. Onishi, P. Jayaram, J. F. Lana and K. Mautner, Platelet-rich plasma: New performance understandings and therapeutic considerations in 2020, *Int. J. Mol. Sci.*, 2020, 1–36, DOI: 10.3390/ijms21207794.

84 T. del Pino-Sedeño, *et al.*, Platelet-rich plasma for the treatment of diabetic foot ulcers: A meta-analysis, *Wound Repair Regen.*, 2019, **27**(2), 170–182, DOI: 10.1111/wrr.12690.
85 M. Rahsaz, B. Geramizadeh, M. Kaviani and S. Marzban, Gelatin for purification and proliferation of primary keratinocyte culture for use in chronic wounds and burns, *Exp. Clin. Transplant. Off. J. Middle East Soc. Organ Transplant.*, 2015, **13**, 361–365.
86 Z. Safari, S. Soudi, N. Jafarzadeh, A. Z. Hosseini, E. Vojoudi and M. Sadeghizadeh, Promotion of angiogenesis by M13 phage and RGD peptide in vitro and in vivo, *Sci. Rep.*, 2019, **9**(1), 11182, DOI: 10.1038/s41598-019-47413-z.
87 A. Y. Kim, Y. Kim, S. H. Lee, Y. Yoon, W. H. Kim and O. K. Kweon, Effect of gelatin on osteogenic cell sheet formation using canine adipose-derived mesenchymal stem cells, *Cell Transplant.*, 2017, **26**(1), 115–123, DOI: 10.3727/096368916X693338.
88 J. W. Park, S. R. Hwang and I. S. Yoon, Advanced growth factor delivery systems in wound management and skin regeneration, *Molecules*, 2017, 1259, DOI: 10.3390/molecules22081259.
89 D. L. Steed, The Role Of Growth Factors In Wound Healing, *Surg. Clin.*, 1997, **77**(3), 575–586, DOI: 10.1016/S0039-6109(05)70569-7.
90 Granulation Tissue - Definition and Function | Biology Dictionary, accessed: Jun. 12, 2024. [Online], available: https://biologydictionary.net/granulation-tissue/#granulation-tissue-definition.
91 C. Ploner, *et al.*, Oxidant therapy improves adipogenic differentiation of adipose-derived stem cells in human wound healing, *Stem Cell Res. Ther.*, 2021, **12**(1), 280, DOI: 10.1186/s13287-021-02336-3.
92 Y. Fukaya, *et al.*, Platelet-rich plasma inhibits the apoptosis of highly adipogenic homogeneous preadipocytes in an in vitro culture system, *Exp. Mol. Med.*, 2012, **44**(5), 330–339, DOI: 10.3858/emm.2012.44.5.037.
93 H. T. Liao, I. B. James, K. G. Marra and J. P. Rubin, The Effects of Platelet-Rich Plasma on Cell Proliferation and Adipogenic Potential of Adipose-Derived Stem Cells, *Tissue Eng., Part A*, 2015, **21**(21–22), 2714–2722, DOI: 10.1089/ten.tea.2015.0159.
94 C. Zhang, *et al.*, Combination of lyophilized adipose-derived stem cell concentrated conditioned medium and polysaccharide hydrogel in the inhibition of hypertrophic scarring, *Stem Cell Res. Ther.*, 2021, **12**(1), 23, DOI: 10.1186/s13287-020-02061-3.
95 H. Cao, J. Wang, Z. Hao and D. Zhao, Gelatin-based biomaterials and gelatin as an additive for chronic wound repair, *Front. Pharmacol.*, 2024, 1398939, DOI: 10.3389/fphar.2024.1398939.
96 Y. Zhang, *et al.*, Ag nanocomposite hydrogels with immune and regenerative microenvironment regulation promote scarless healing of infected wounds, *J. Nanobiotechnol.*, 2023, **21**(1), 435, DOI: 10.1186/s12951-023-02209-2.
97 M. Plotczyk and F. Jimenez, Hair Follicles in Wound Healing and Skin Remodelling, in *Hair Follicle Regeneration*, F. Jimenez and C. Higgins, Springer International Publishing, 2022, pp. 291–304.
98 M. Zhu, *et al.*, Platelet sonicates activate hair follicle stem cells and mediate enhanced hair follicle regeneration, *J. Cell. Mol. Med.*, 2020, **24**(2), 1786–1794, DOI: 10.1111/jcmm.14873.